

This is the **Accepted Version** of a paper published in the journal: International Journal of Heat and Mass Transfer

Inam, Mohammad Ilias, Lin, Wenxian, Armfield, S.W., and He, Yinghe (2015) *Asymmetry and penetration of transitional plane fountains in stratified fluid*. International Journal of Heat and Mass Transfer, 90. pp. 1125-1142.

<http://dx.doi.org/http://dx.doi.org/10.1016/j.ijheatmasstransfer.2015.07.062>

Asymmetry and penetration of transitional plane fountains in stratified fluid

Mohammad Ilias Inam^a, Wenxian Lin^{1a,b}, S. W. Armfield^c, Yinghe He^a

^a*College of Science, Technology & Engineering, James Cook University,
Townsville, QLD 4811, Australia*

^b*Solar Energy Research Institute, Yunnan Normal University,
Kunming, Yunnan 650092, P. R. China*

^c*School of Aerospace, Mechanical and Mechatronic Engineering,
The University of Sydney, NSW 2006, Australia*

Abstract

Fountains injected into stratified fluids are widely found in **environmental and industrial** settings. The onset of asymmetry and entrainment that occurs in transitional fountains is the key to understanding turbulence generation and entrainment mechanisms in fountains. In addition to the Reynolds number (Re) and the Froude number (Fr), the stratification of the ambient fluid, represented by the dimensionless temperature stratification parameter (s), also has a significant effect on the onset of asymmetry, unsteadiness, and entrainment **in a fountain, and on the maximum height** that the fountain penetrates in the ambient fluid. In this study, a series of three-dimensional direct numerical simulations (DNS) were carried out using ANSYS Fluent for transitional plane fountains in linearly-stratified fluids with Re and s in the ranges of $25 \leq Re \leq 300$ and $0 \leq s \leq 0.5$, all at $Fr = 10$. The transient behaviour of the fountains, in particular the effects of Re and s on the asymmetric transition and the maximum fountain penetration heights, is analysed and quantified using the DNS results. It is found that fountains are generally symmetric in the early developing stage, but become asymmetric and unsteady subsequently. The stratification of the ambient fluid is shown to stabilize the fountain flow and to reduce its asymmetry and unsteadiness. However, the effect of s on the asymmetric behaviour of a fountain is found to be weaker than that of Re . Empirical correlations were developed, using the numerical results, to quantify such effects on the time for the asymmetric transi-

¹Corresponding author: Email: wenxian.lin@jcu.edu.au, Phone: +61-7-4781-5091, Fax: +61-7-4781-6788 (W. Lin)

tion. The effects of Re and s on the initial and time-averaged maximum fountain heights ($z_{m,i}$ and $z_{m,a}$, respectively), and the time to attain $z_{m,i}$ are also analysed. Quantified correlations are developed using the DNS results, which demonstrate that both $z_{m,i}$ and $z_{m,a}$ increase with Re , but decrease with s , apparently due to the increasing negative buoyancy that the fountain must overcome to penetrate the ambient fluid. The results further show that the effect of s on $z_{m,i}$ and $z_{m,a}$ is much stronger than that of Re .

Keywords: Direct numerical simulation, Plane fountain, Asymmetry, Stratification, Transitional flow, Maximum fountain height.

1. Introduction

Fountains are abundant in nature and in many industrial and environmental settings, such as natural ventilation, volcanic eruptions, cumulus clouds, reverse cycle air-conditioning, to name just a few. A fountain occurs whenever a denser fluid is injected vertically upward into a less dense fluid or a less dense fluid is injected vertically downward into a denser fluid. In both cases buoyancy opposes the momentum of the jet flow, leading to gradually reduced vertical jet velocity until it becomes zero at a certain finite height. After that, the jet flow reverses its direction and comes back around the core of the upward or downward flow and an intrusion forms on the base which moves outwards.

When **injected** into a homogeneous ambient fluid, the behavior of a fountain is governed by the Reynolds number, Re , and the Froude number, Fr , defined as follows,

$$Re = \frac{W_0 X_0}{\nu}, \quad (1)$$

$$Fr = \frac{W_0}{[gX_0(\rho_0 - \rho_a)/\rho_a]^{1/2}} = \frac{W_0}{[g\beta X_0(T_a - T_0)]^{1/2}}, \quad (2)$$

where X_0 is the radius of the orifice at the fountain source for a round fountain or the half-width of the slot at the source for a plane fountain, W_0 is the mean inlet velocity of the jet fluid at the source, g is the acceleration due to gravity, ρ_0 , T_0 and ρ_a , T_a are the densities and temperatures of the jet fluid and the ambient fluid at the source, and ν and β are the kinematic viscosity and coefficient of volumetric expansion of fluid, respectively. The second expression of Fr applies when the density difference is due to the difference in temperatures of the jet and ambient fluids using the Oberbeck-Boussinesq approximation.

When the ambient fluid is linearly stratified, the fountain behaviour will also depend on the density stratification parameter, S_p , which is defined as,

$$S_p = -\frac{1}{\rho_{a,0}} \frac{d\rho_{a,Z}}{dZ}, \quad (3)$$

where $\rho_{a,0}$ and $\rho_{a,Z}$ are the initial densities of the ambient fluid at the bottom (*i.e.*, at $Z = 0$) and at the height Z , with Z being the coordinate in the vertical direction as sketched in Fig. 1, which depicts the physical system under consideration and the coordinates used in this paper. If the Oberbeck-Boussinesq approximation is valid, S_p can also be represented by the following temperature stratification parameter, S ,

$$S = \frac{dT_{a,Z}}{dZ} = \frac{S_p}{\beta}, \quad (4)$$

where $T_{a,Z}$ is the initial temperature of the ambient fluid at Z . However, the dimensionless form of S , as defined below, is normally used instead,

$$s = \frac{d\theta_{a,z}}{dz} = \frac{X_0}{(T_{a,0} - T_0)} S = \frac{X_0}{\beta(T_{a,0} - T_0)} S_p, \quad (5)$$

where $\theta_{a,z} = (T_{a,Z} - T_{a,0})/(T_{a,0} - T_0)$ and $z = Z/X_0$ are the dimensionless initial temperature of the ambient fluid at Z and the dimensionless height, respectively, and $T_{a,0}$ is the initial temperature of the ambient fluid at the bottom, *i.e.*, at $Z = 0$.

Although studies on fountains commenced in the 1950s (see, *e.g.*, [1]), they are still being extensively investigated (see, *e.g.*, [2–12]). However, the studies have focused on round fountains, which may be either ‘very weak’ when $Fr \lesssim 1$, or ‘weak’ when $1 \lesssim Fr \lesssim 3$, or ‘forced’ when $Fr \gtrsim 3$, as classified by Kaye and Hunt[13] and Burrige and Hunt [7]. The behavior of a forced round fountain is found to be significantly different from that of a weak or very weak round fountain, as summarized in, *e.g.*, [7, 13–16]. For example, in a forced round fountain, z_m , which is the dimensionless maximum height that the fountain will penetrate in a homogeneous ambient fluid (nondimensionalized by X_0), is proportional to Fr and has no dependence on Re , as found by numerous studies (*e.g.*, [4–8, 13, 17–26]), whereas in a weak or very weak round fountain, due to the weaker discharge momentum flux compared to the negative buoyancy flux, z_m is also strongly dependent on Re , in addition to its dependence on Fr , as noted, *e.g.*, by Lin and Armfield [14, 27–29], Philippe *et al.* [30], and Williamson *et al.* [15]. Williamson *et al.* [15] then proposed to

classify a round fountain in terms of its Re as well, *i.e.*, a ‘laminar’ round fountain when $Re < 120$, a ‘transitional’ round fountain when $120 < Re < 2000$, and a ‘turbulent’ round fountain when $Re > 2000$, based on their extensive experimental observations. Such fountains are common in a number of settings. Specific examples are very weak fountains used for the replenishing of cold salt water at the bottom of solar ponds [31]; weak and forced fountains dominating in building ventilation when cool air is injected vertically into a room through vents in the floor, with typical values of Fr and Re in the ranges $1 \leq Fr \leq 25$ and $100 \leq Re \leq 1000$, as estimated by Burrige, Mistry and Hunt [32]; and forced fountains occurring in volcanic eruptions [20]. Many more examples of very weak, weak and forced fountains can be found in environmental, geophysical, and atmospheric settings and in industrial applications (see, *e.g.*, [16, 18, 22, 26, 33]).

The behavior of plane fountains, which are formed by injecting upwards continuously a denser fluid into a homogeneous light ambient fluid from a long narrow slot, is also investigated by some researchers, as summarized recently in [9, 34], although apparently not so extensively as round fountains. For turbulent plane fountains, it was found that, similar to forced round fountains, z_m is also independent of Re ; however, its dependence on Fr is in the form $z_m \sim Fr^{4/3}$, as obtained by, *e.g.*, [20, 21, 35–37], although other forms were also proposed (*e.g.*, [36–38]). For example, Hunt and Coffey [36] found that $z_m \sim Fr^2$ for weak plane fountains with $2.3 \lesssim Fr \lesssim 5.7$, but it becomes $z_m \sim Fr^{2/3}$ for very weak plane fountains, which is the same as that obtained by Lin and Armfield [28].

For laminar and transitional plane fountains, similar to their counterpart round fountains, Re also affects z_m , as demonstrated by Lin and Armfield [29, 39] who gave the following scaling based on dimensional and scaling analysis,

$$z_m \sim \frac{Fr}{Re^{1/2}}, \quad (6)$$

which was confirmed by their DNS results for $0.2 \leq Fr \leq 1$ and $5 \leq Re \leq 800$. This scaling was also confirmed by a recent experimental study by Srinarayana *et al.* [3] for $2.1 \lesssim Re \lesssim 127$ and $0.4 \lesssim Fr \lesssim 42$.

The onset of asymmetry, instability and unsteadiness in fountains is the key to elucidating the mechanism for the generation of turbulence and entrainment in fountains, but is not well understood, although some recent investigations have been undertaken,

as follows. Lin and Armfield [14] studied the onset of entrainment in transitional round fountains in a homogeneous fluid over the ranges of $1 \leq Fr \leq 8$ and $200 \leq Re \leq 800$ using DNS, and found that entrainment is strongly dependent on Re while the effect of Fr is much smaller. Williamson et al. [2] investigated the transitional behaviour of weak turbulent round fountains in a homogeneous fluid over a wide range of Re (20 to 3494), although Fr was relatively small with $0.1 \leq Fr \leq 2.1$. They observed that there is a continuum of behaviour over this transitional Fr range, from hydraulically driven buoyancy dominated flow to momentum dominated flow. Srinarayana *et al.* [3] investigated the plane fountain behavior at low-Reynolds numbers using a series of experiments for $2.1 \lesssim Re \lesssim 127$ and $0.4 \lesssim Fr \lesssim 42$ and found that the behavior of plane fountains can be categorized broadly into four regimes: the steady; flapping; laminar mixing; and jet-type mixing behavior. It was also found that the critical Froude number for transition from a steady to unsteady flow varies with Re . Srinarayana *et al.* [9, 40] also conducted a series of two-dimensional DNS of laminar plane fountains in homogeneous ambient fluids with both a uniform and a parabolic inlet velocity profile at the fountain source, to study the instabilities and variation of the fountain height and obtained the critical Froude number for unsteadiness at full development. More recently, Gao et al. [41] used three-dimensional DNS results to explore the asymmetry and three-dimensionality in transitional round fountains in a linearly stratified fluid over the ranges of $1 \leq Fr \leq 8$ and $100 \leq Re \leq 500$ at a constant dimensionless stratification $s = 0.03$. Their results show that a critical Re exists between 100 and 200 for $Fr = 2$ fountains, and similarly a critical Fr exists between 1 and 2 for fountains at $Re = 200$, which divide the fountains into either axisymmetric and two-dimensional or asymmetric and three-dimensional. Both Williamson et al. [2] and Gao et al. [41] investigated the behavior of round transitional fountains for relatively small Fr values. No study has been found in which the onset of asymmetry in transitional plane fountains in stratified fluids has been investigated, which motivates the current study.

In this study, a series of three-dimensional DNS runs were carried out for transitional plane fountains in linearly stratified fluids over the ranges of $25 \leq Re \leq 300$ and $0 \leq s \leq 0.5$ at a constant high Froude number of $Fr = 10$ to demonstrate the effect of Re and s on the onset of asymmetry, instability and unsteadiness of these plane fountains.

The remainder of this paper is organized as follows. The physical system under consid-

eration, the governing equations and the initial and boundary conditions for the flow, and the numerical methods for DNS are briefly described in § 2. The asymmetric transition of the $Fr = 10$ plane fountains over the ranges of $25 \leq Re \leq 300$ and $0 \leq s \leq 0.5$ is described and discussed in § 3, both qualitatively and quantitatively, with the DNS results. In § 4, the initial and time-averaged maximum fountain penetration height, as well as the time to attain the initial maximum fountain height, are analysed and quantified with the DNS results. Finally, the conclusions are drawn in § 5.

2. Methodology

The physical system under consideration is a rectangular container of the dimensions $H \times B \times L$ (Height \times Width \times Length), containing a Newtonian fluid initially at rest and with a constant temperature gradient $dT_{a,z}/dZ$, as sketched in Fig. 1. At the center of the bottom of the container, a narrow slot with a half-width of X_0 in the Y direction functions as the source for a plane fountain, with the remainder of the bottom being a rigid non-slip and adiabatic boundary. The two vertical surfaces in the $X - Z$ plane, at $Y = \pm B/2$, are assumed to be periodic whereas the two vertical surfaces in the $Y - Z$ plane, at $X = \pm L/2$, are assumed to be outflows. The top surface in the $X - Y$ plane, at $Y = H$, is also assumed to be an outflow. The origin of the Cartesian coordinate systems is at the center of the bottom. **The gravity is acting in the negative Z -direction.** At time $t = 0$, a stream of fluid at T_0 ($T_0 < T_{a,0}$) is injected upward from the slot with a uniform velocity W_0 into the container to initiate the plane fountain flow and this discharge is maintained over the whole course of a specific DNS run.

The flow is governed by the three-dimensional incompressible Navier-Stokes and temperature equations with the Oberbeck-Boussinesq approximation, which are written in conservative form in Cartesian coordinates as follows,

$$\frac{\partial U}{\partial X} + \frac{\partial V}{\partial Y} + \frac{\partial W}{\partial Z} = 0, \quad (7)$$

$$\frac{\partial U}{\partial t} + \frac{\partial(UU)}{\partial X} + \frac{\partial(VU)}{\partial Y} + \frac{\partial(WU)}{\partial Z} = -\frac{1}{\rho} \frac{\partial P}{\partial X} + \nu \left(\frac{\partial^2 U}{\partial X^2} + \frac{\partial^2 U}{\partial Y^2} + \frac{\partial^2 U}{\partial Z^2} \right), \quad (8)$$

$$\frac{\partial V}{\partial t} + \frac{\partial(UV)}{\partial X} + \frac{\partial(VV)}{\partial Y} + \frac{\partial(WV)}{\partial Z} = -\frac{1}{\rho} \frac{\partial P}{\partial Y} + \nu \left(\frac{\partial^2 V}{\partial X^2} + \frac{\partial^2 V}{\partial Y^2} + \frac{\partial^2 V}{\partial Z^2} \right), \quad (9)$$

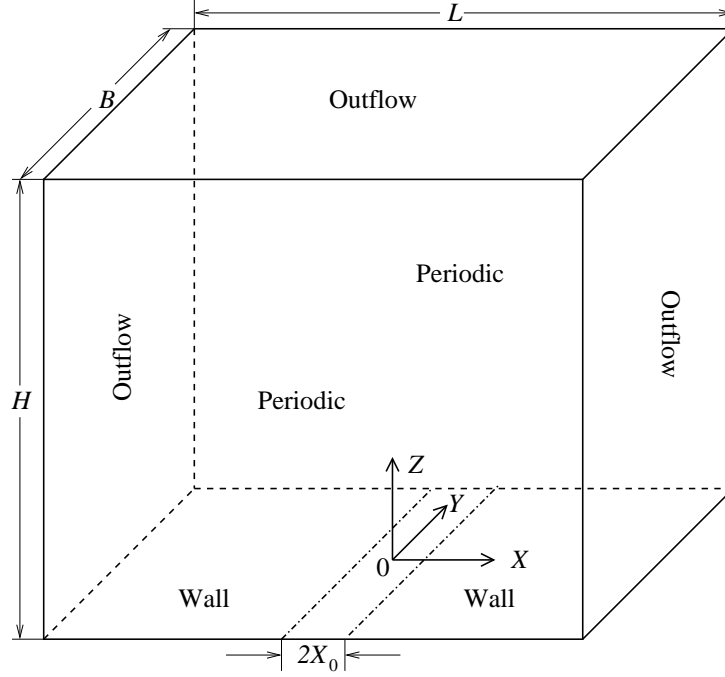


Figure 1: Sketch of the physical system under consideration, the computational domain and the boundary conditions.

$$\frac{\partial W}{\partial t} + \frac{\partial(UW)}{\partial X} + \frac{\partial(VW)}{\partial Y} + \frac{\partial(WW)}{\partial Z} = -\frac{1}{\rho} \frac{\partial P}{\partial Z} + \nu \left(\frac{\partial^2 W}{\partial X^2} + \frac{\partial^2 W}{\partial Y^2} + \frac{\partial^2 W}{\partial Z^2} \right) + g\beta(T - T_{a,z}), \quad (10)$$

$$\frac{\partial T}{\partial t} + \frac{\partial(UT)}{\partial X} + \frac{\partial(VT)}{\partial Y} + \frac{\partial(WT)}{\partial Z} = \kappa \left(\frac{\partial^2 T}{\partial X^2} + \frac{\partial^2 T}{\partial Y^2} + \frac{\partial^2 T}{\partial Z^2} \right), \quad (11)$$

where U , V , and W are the velocity components in the X , Y , and Z directions, t is time, P is pressure, T is temperature, and ρ , ν , and κ are the density, viscosity, and thermal diffusivity of fluid, respectively.

The appropriate initial and boundary conditions are:

$$U = V = W = 0, \quad T(Z) = T_{a,0} + s(T_{a,0} - T_0) \frac{Z}{X_0} \text{ at all } X, Y, Z$$

when $t < 0$, and

$$U = V = 0, \quad W = W_0, \quad T = T_0 \text{ at } Z = 0, \quad -X_0 \leq X \leq X_0 \text{ and } -\frac{B}{2} \leq Y \leq \frac{B}{2};$$

$$U = V = W = 0, \quad \frac{\partial T}{\partial Z} = 0 \text{ at } Z = 0, \quad X_0 \leq X \leq \frac{L}{2} \text{ and } -\frac{B}{2} \leq Y \leq \frac{B}{2};$$

$$\begin{aligned}
U = V = W = 0, \quad \frac{\partial T}{\partial Z} = 0 \text{ at } Z = 0, \quad -\frac{L}{2} \leq X \leq -X_0 \text{ and } -\frac{B}{2} \leq Y \leq \frac{B}{2}; \\
\frac{\partial U}{\partial Z} = \frac{\partial V}{\partial Z} = \frac{\partial W}{\partial Z} = \frac{\partial T}{\partial Z} = 0 \text{ at } Z = H, \quad -\frac{L}{2} \leq X \leq \frac{L}{2} \text{ and } -\frac{B}{2} \leq Y \leq \frac{B}{2}; \\
\frac{\partial U}{\partial X} = \frac{\partial V}{\partial X} = \frac{\partial W}{\partial X} = \frac{\partial T}{\partial X} = 0 \text{ at } X = \pm \frac{L}{2}, \quad -\frac{B}{2} \leq Y \leq \frac{B}{2} \text{ and } 0 \leq Z \leq H; \\
U(Y = \frac{B}{2}) = U(Y = -\frac{B}{2}), \quad V(Y = \frac{B}{2}) = V(Y = -\frac{B}{2}), \quad W(Y = \frac{B}{2}) = W(Y = -\frac{B}{2}), \\
T(Y = \frac{B}{2}) = T(Y = -\frac{B}{2}) \text{ at } -\frac{L}{2} \leq X \leq \frac{L}{2} \text{ and } 0 \leq Z \leq H
\end{aligned}$$

when $t > 0$.

The above governing equations were discretized on a non-uniform rectangular mesh using a finite volume method, with a standard 2nd-order central difference scheme used for the viscous and divergence terms and the 3rd-order QUICK scheme for the advection terms. The 2nd-order Adams-Bashforth and Crank-Nicolson schemes were used for the time integration of the advective and diffusive terms, respectively. The PRESTO (PREssure STaggering Option) scheme was used for the pressure gradient.

There are totally 30 DNS runs carried out in this study using ANSYS Fluent 13, with the key information about these runs listed in Table 1. **The fluid used in the DNS runs is water, with the density $\rho_a = 996.6 \text{ kg/m}^3$, the kinematic viscosity $\nu = 8.58 \times 10^{-7} \text{ m}^2/\text{s}$, and the volume expansion coefficient $\beta = 2.76 \times 10^{-4} \text{ 1/K}$, respectively, at the nominal temperature of $T_{a,0} = 300 \text{ K}$. These thermal property values were obtained by interpolating the data presented in Table A-3 of [42], and were used for all DNS runs. The maximum value of $(T_{a,0} - T_0)$, among all DNS runs, is $(300 - 298.0428) = 1.9572 \text{ K}$, which is small enough to ensure the Oberbeck-Boussinesq approximation is valid. The temperatures or temperature differences such as 298.0428 K or 1.9572 K are calculated for water from the definitions of Re and Fr with the Oberbeck-Boussinesq approximation. Such temperatures around 300 K correspond to the common room temperatures. Although these temperatures or their differences are stated to 4 decimal places in order the targeted specific Re and Fr values to be accurately set, which are easily achievable for numerical simulations, it is understood that in an experimental context it is not possible to measure to that degree of precision. For all DNS runs, Fr is fixed at 10, $T_{a,0}$ is fixed at 300 K, the time step is fixed at 0.025 s, but Re and s vary in the ranges of $25 \leq Re \leq 300$ and $0.1 \leq s \leq 0.5$, respectively. In addition, the DNS runs with $s = 0$, which corresponds**

to a homogeneous fluid case, were also carried out for the purpose of comparison. Non-uniform meshes were used, with total numbers of cells in the range of 3.72 to 6.67 million. In the regions of $-15 \leq X/X_0 \leq 15$, $0 \leq Z/X_0 \leq 45$ and $-150 \text{ mm} \leq Y \leq 150 \text{ mm}$, a uniform and finer rectangular mesh was used, and in the remaining regions a relatively coarse and non-uniform mesh with varying expansion rates was used. It should be noted that “outflows” boundary conditions are applied at the lateral boundaries of the domain (in the X -direction, *i.e.*, at the locations $X = \pm L/2$), which assumes a zero diffusion flux for all flow variables. Such a zero diffusion flux condition applied by Fluent at “outflow” boundaries is approached physically in fully-developed flows. The “outflow” boundaries can also be defined at physical boundaries where the flow is not fully developed if the assumption of a zero diffusion flux at the exit is expected to have a negligible impact on the flow solution. In all DNS runs, H , B and L were chosen to be sufficiently large to ensure that the “outflows” and periodic boundary conditions have negligible effect on the flow quantities of interest.

Table 1: Key information about the DNS runs.

| Re (-) | s (-) | X_0 (m) | W_0 (m/s) | T_0 (K) | S (K/m) | $H \times B \times L$ (m×m×m) | Grids (million) |
|-------------|------------|--------------|----------------|--------------|--------------|----------------------------------|--------------------|
| 25 | 0 | 0.002 | 0.01072 | 299.7876 | 0.0 | 0.215×0.3×0.8 | 3.72 |
| 25 | 0.1 | 0.002 | 0.01072 | 299.7876 | 10.6 | 0.172×0.3×0.8 | 3.72 |
| 25 | 0.2 | 0.002 | 0.01072 | 299.7876 | 21.2 | 0.172×0.3×0.8 | 3.72 |
| 25 | 0.3 | 0.002 | 0.01072 | 299.7876 | 31.9 | 0.172×0.3×0.8 | 3.72 |
| 25 | 0.4 | 0.002 | 0.01072 | 299.7876 | 42.5 | 0.172×0.3×0.8 | 3.72 |
| 25 | 0.5 | 0.002 | 0.01072 | 299.7876 | 53.1 | 0.172×0.3×0.8 | 3.72 |
| 50 | 0 | 0.002 | 0.02145 | 299.1505 | 0.0 | 0.215×0.3×0.8 | 3.72 |
| 50 | 0.1 | 0.002 | 0.02145 | 299.1505 | 42.5 | 0.172×0.3×0.8 | 3.72 |
| 50 | 0.2 | 0.002 | 0.02145 | 299.1505 | 85.0 | 0.172×0.3×0.8 | 3.72 |
| 50 | 0.3 | 0.002 | 0.02145 | 299.1505 | 127.4 | 0.172×0.3×0.8 | 3.72 |
| 50 | 0.4 | 0.002 | 0.02145 | 299.1505 | 169.9 | 0.172×0.3×0.8 | 3.72 |
| 50 | 0.5 | 0.002 | 0.02145 | 299.1505 | 212.4 | 0.172×0.3×0.8 | 3.72 |
| 100 | 0 | 0.003 | 0.02860 | 298.9932 | 0.0 | 0.325×0.3×0.8 | 5.77 |
| 100 | 0.1 | 0.003 | 0.02860 | 298.9932 | 33.6 | 0.260×0.3×0.8 | 5.77 |
| 100 | 0.2 | 0.003 | 0.02860 | 298.9932 | 67.1 | 0.260×0.3×0.8 | 5.77 |
| 100 | 0.3 | 0.003 | 0.02860 | 298.9932 | 100.7 | 0.260×0.3×0.8 | 5.77 |
| 100 | 0.4 | 0.003 | 0.02860 | 298.9932 | 134.2 | 0.260×0.3×0.8 | 5.77 |

| | | | | | | | |
|-----|-----|-------|---------|----------|-------|---------------|------|
| 100 | 0.5 | 0.003 | 0.02860 | 298.9932 | 167.8 | 0.260×0.3×0.8 | 5.77 |
| 200 | 0 | 0.005 | 0.03432 | 299.1301 | 0.0 | 0.535×0.3×0.8 | 6.67 |
| 200 | 0.1 | 0.005 | 0.03432 | 299.1301 | 17.4 | 0.430×0.3×0.8 | 6.67 |
| 200 | 0.2 | 0.005 | 0.03432 | 299.1301 | 34.8 | 0.430×0.3×0.8 | 6.67 |
| 200 | 0.3 | 0.005 | 0.03432 | 299.1301 | 52.2 | 0.430×0.3×0.8 | 6.67 |
| 200 | 0.4 | 0.005 | 0.03432 | 299.1301 | 69.6 | 0.430×0.3×0.8 | 6.67 |
| 200 | 0.5 | 0.005 | 0.03432 | 299.1301 | 87.0 | 0.430×0.3×0.8 | 6.67 |
| 300 | 0 | 0.006 | 0.05148 | 298.0428 | 0.0 | 0.645×0.1×0.8 | 4.45 |
| 300 | 0.1 | 0.005 | 0.05148 | 298.0428 | 39.1 | 0.430×0.3×0.8 | 6.67 |
| 300 | 0.2 | 0.006 | 0.04290 | 298.8673 | 37.8 | 0.516×0.1×0.8 | 4.45 |
| 300 | 0.3 | 0.006 | 0.04290 | 298.8673 | 56.6 | 0.516×0.1×0.8 | 4.45 |
| 300 | 0.4 | 0.006 | 0.04290 | 298.8673 | 75.5 | 0.516×0.1×0.8 | 4.45 |
| 300 | 0.5 | 0.006 | 0.04290 | 298.8673 | 94.4 | 0.516×0.1×0.8 | 4.45 |

Extensive mesh and time-step dependency testing was carried out to ensure accurate simulations have been produced. The results of one example of such a test are presented in Fig. 2 for the case of $Fr = 10$, $Re = 50$ and $s = 0.1$, which shows the time series of the maximum fountain height (Z_m) and the horizontal temperature and vertical velocity profiles at the height of $Z = 0.015$ m on the vertical plane at $Y = 0$ m. Z_m was determined as the vertical distance from the bottom to the vertex point of the iso-surface at the temperature of $T(Z) = T_0 - 1\%(T_{a,0} - T_0)$ within the whole computational domain. These results were obtained numerically with three different meshes, with the coarse mesh having 2.39 million cells, the basic mesh having 3.72 million cells and the fine mesh having 5.27 million cells, and at three different time steps of 0.025 s, 0.035 s, and 0.05 s, respectively. It is clear from Fig. 2(a)-(c), where a comparison of the results obtained with the three meshes, all at the same time-step of 0.025 s, is presented, that the results obtained with the basic mesh and the fine mesh are essentially the same and only the results produced with the coarse mesh have some noticeable deviations. Similarly, a comparison of the results obtained with three time steps, all with the same basic mesh (3.72 million cells), as shown in Fig. 2(d)-(f), shows that the differences are very small. Hence it is believed that the combination of the basic mesh with 3.72 million cells and the time step at 0.025 s produces sufficiently accurate solutions and is the best compromise between the accuracy and the time and computing resources among the meshes and time steps considered, and is then chosen as the main mesh and time step for the numerical simulations at small Re

($Re \leq 50$). For larger Re cases, the mesh and time-step dependency tests found that finer meshes, ranging from 4.45 to 6.67 million cells, as presented in Table 1, all at the time step of 0.025 s, are needed to produce sufficiently accurate solutions. For a typical DNS run, it usually took 10 \sim 18 days on a Dell OptiPlex(TM) 9010 MT desktop computer with Intel Core i7-3770 Processor, 8M Cache, 3.90 GHz, and 32GB DDR3 SDRAM Memory.

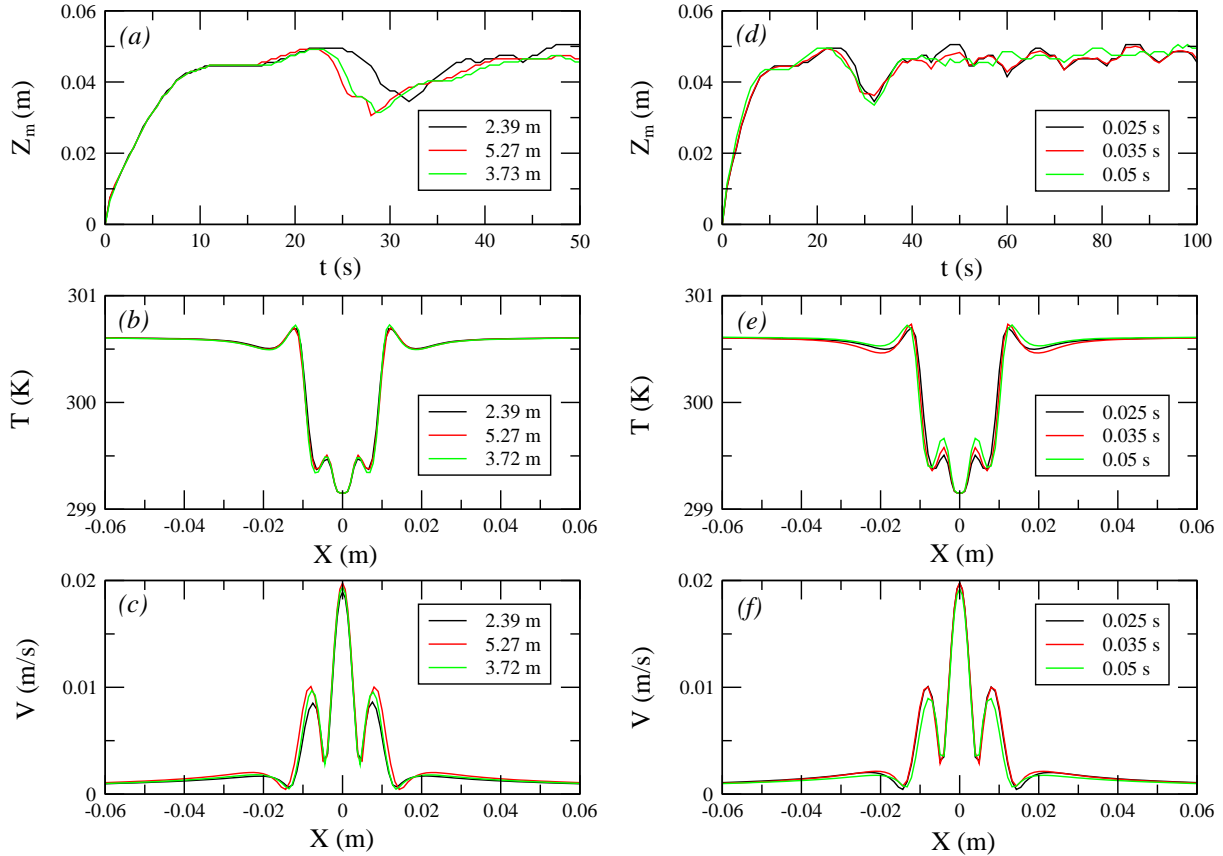


Figure 2: The time series of the maximum fountain height (Z_m) and the horizontal temperature and vertical velocity profiles at $t = 10$ s at the height $Z = 0.015$ m on the vertical plane at $Y = 0$ m, which were obtained numerically for the case of $Fr = 10$, $Re = 50$ and $s = 0.1$ with three different meshes (left column, all at the same time step of 0.025 s) and at three different time steps (right column, all with the same basic mesh of 3.72 million cells).

3. Asymmetric transition

3.1. Qualitative observations

3.1.1. Evolution of transient temperature and velocity fields

Figure 3 presents the transient temperature contours of a typical plane fountain with $Fr = 10$, $Re = 100$ and $s = 0.1$ at the instants of $\tau = 25, 120, 145, 165, 260$, and 570 , respectively, on three specific planes in each of the X , Y , and Z directions, where τ is the dimensionless time, made dimensionless by X_0/W_0 . The results show that at $Y = 0$ in the $X - Z$ plane the fountain flow maintains symmetry in the $X - Z$ plane with respect to $X = 0$ at its early development stage, until at $\tau \approx 165$, when it starts to become asymmetric and unstable, leading to flapping motions (*i.e.*, the horizontal oscillations) around $X = 0$ in the X direction. The transition from a symmetric flow to an asymmetric one in the Y direction in the $Y - Z$ plane occurs at a later time, as the temperature contours at $X = 0$ in the $Y - Z$ plane demonstrate that the fountain height is basically the same along the Y direction for each time instant until $\tau \approx 260$, when the height is observed to fluctuate along the Y direction, indicating that the symmetry has collapsed and the fountain has become asymmetric in the Y direction. This is also true in the horizontal, $X - Y$ plane, as the temperature contours at $Z = 10X_0$ in the $X - Y$ plane show that the fountain width at this specific height is essentially the same in the X direction for each time instant until $\tau \approx 260$, when the width varies considerably along the X direction, confirming that the symmetry collapses and the fountain becomes asymmetric in the Y direction of the $X - Y$ plane. The behavior of the fountain flow becomes quasi-steady at the later development stage because the time-averaged behavior essentially attains a steady state, although the instantaneous behaviour still changes with time.

The onset of asymmetry and unsteady behaviour, observed above in the temperature fields, is also exhibited by the corresponding transient velocity contours, as shown in Fig. 4 where the transient contours of U/W_0 and V/W_0 at $X = 0$ in the $Y - Z$ plane are presented. When a plane fountain maintains symmetry with respect to $X = 0$ in the $X - Z$ plane, U should be zero everywhere at $X = 0$ in the $Y - Z$ plane. Any non-zero U value on this plane will indicate asymmetric behaviour in the X direction. Similarly,

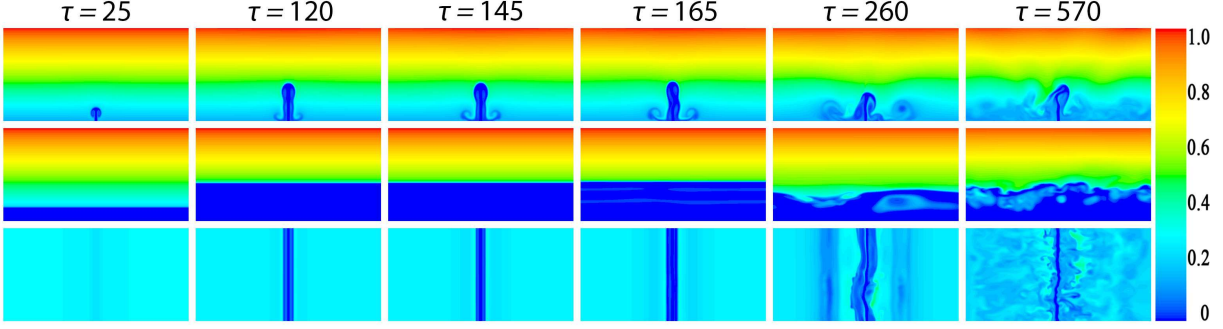


Figure 3: Evolution of transient temperature contours of the plane fountain with $Fr = 10$, $Re = 100$ and $s = 0.1$ at $Y = 0$ in the $X - Z$ plane (top row), $X = 0$ in the $Y - Z$ plane (middle row), and $Z = 10X_0$ in the $X - Y$ plane (bottom row), respectively. The temperature contours in each subfigure are normalized with $[T(Z) - T_0]/(T_{a,Z=60X_0} - T_0)$.

when a plane fountain maintains **symmetry** in the Y direction on the $Y - Z$ plane, V should be zero everywhere at $X = 0$ in the $Y - Z$ plane. Any non-zero V on this plane will indicate **asymmetric** behaviour in the Y direction. From Fig. 4, it is clearly seen that when $\tau \leq 120$, both U/W_0 and V/W_0 are zero, indicating that **symmetry** is maintained both in the X direction in the $X - Z$ plane and in the Y direction in the $Y - Z$ plane. At $\tau \approx 145$, significant asymmetric features are observed in the X direction in the $X - Z$ plane and the extent of the asymmetry increases when τ is further increased. At $\tau \approx 165$, marginal asymmetric features are shown in the Y direction in the $Y - Z$ plane and the extent of the asymmetry also increases for large τ , although the magnitude of the asymmetry in the Y direction is much smaller than that in the X direction at the corresponding time instants.

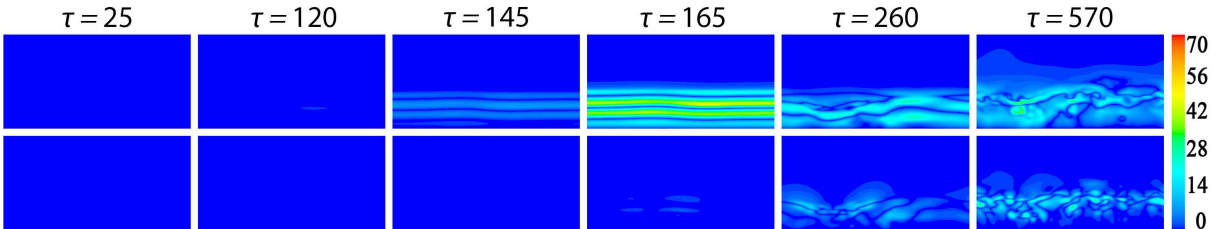


Figure 4: Evolution of transient contours of U/W_0 (top row) and V/W_0 (bottom row), both in percentage, at $X = 0$ in the $Y - Z$ plane for the plane fountain with $Fr = 10$, $Re = 100$ and $s = 0.1$.

3.1.2. Effect of Re

The effect of Re on the asymmetric and unsteady behaviour of plane fountains is demonstrated in Fig. 5 where representative temperature contours at the quasi-steady state on three individual planes with Re varying in the range $25 \leq Re \leq 300$, all with $Fr = 10$ and $s = 0.1$ are shown. The results show that at the quasi-steady state all these plane fountains become asymmetric and unsteady. The fountain flow in the $X - Z$ plane flaps in the X direction and the fountain heights at higher Re values (200 and 300) are considerably larger than those at smaller Re values. It is also observed that the extent of entrainment increases with Re . In the $Y - Z$ plane, the increase of Re leads to larger fluctuations of the fountain height along the Y direction. Similarly, the increase in Re results in a larger fountain width and increased fluctuation of the width in the $X - Y$ plane as well.

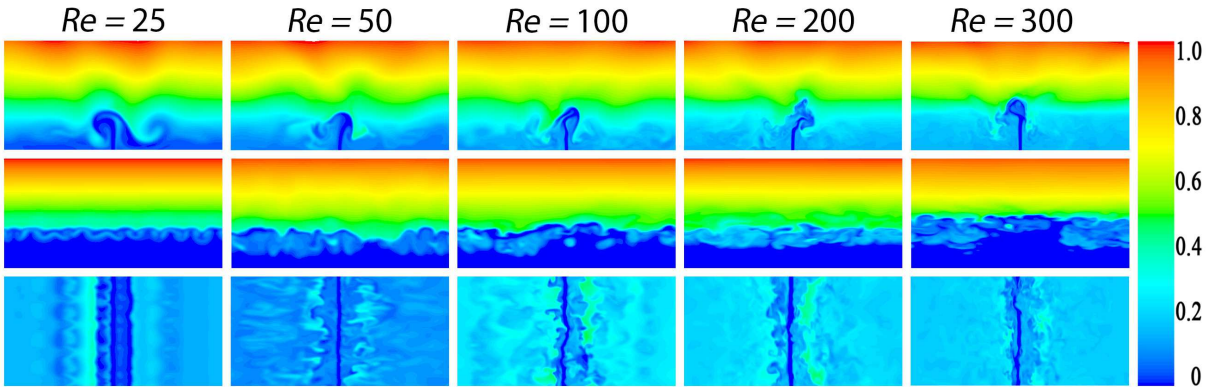


Figure 5: Representative temperature contours of plane fountains at the quasi-steady state for different Re values with $Fr = 10$ and $s = 0.1$ at $Y = 0$ in the $X - Z$ plane (top row), $X = 0$ in the $Y - Z$ plane (middle row), and $Z = 0.5Z_{m,i}$ in the $X - Y$ plane (bottom row), respectively, where $Z_{m,i}$ is the initial maximum fountain height.

Figure 6 presents the corresponding representative contours of U/W_0 and V/W_0 at the quasi-steady **stage** at $X = 0$ in the $Y - Z$ plane for the same plane fountains as for Fig. 5. It is seen that non-zero U values are present at $X = 0$ in the $Y - Z$ plane, indicating that the fountain flow in the $X - Z$ plane flaps in the X direction, which is in agreement with the observation from the temperature contours shown in Fig. 5 and confirms that all these plane fountains become asymmetric and unsteady. It is further observed that

the extent of flapping and entrainment increases when Re increases. In the Y direction of the $Y - Z$ plane, the increase in Re leads to an increased non-zero V value, although the magnitude is smaller than that of the corresponding U value, indicating an increasing extent of asymmetric behaviour in this direction.

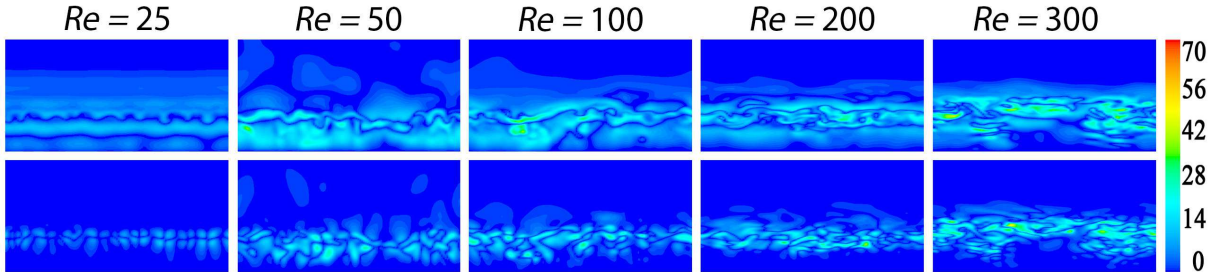


Figure 6: Representative contours of U/W_0 (top row) and V/W_0 (bottom row) of plane fountains at the quasi-steady stage for different Re values with $Fr = 10$ and $s = 0.1$ at $X = 0$ in the $Y - Z$ plane, where U/W_0 and V/W_0 are in percentage.

A more evident demonstration of the effect of Re on the asymmetric behaviour of plane fountains in both the X and Y directions of the $Y - Z$ plane is presented in Fig. 7, where the time series of U_{max}/W_0 and V_{max}/W_0 at $X = 0$ in the $Y - Z$ plane with Re varying in the range $25 \leq Re \leq 300$, all at $Fr = 10$ and $s = 0.1$, are presented. U_{max} and V_{max} represent the maximum values of U and V at $X = 0$ in the $Y - Z$ plane, respectively. From this figure, it is seen that both U_{max}/W_0 and V_{max}/W_0 are essentially zero at the early developing stage for all cases considered, indicating that these plane fountains are initially symmetric in both the X and Y directions. However, subsequently all fountains under consideration exhibit asymmetric behaviour, with their U_{max}/W_0 and V_{max}/W_0 values becoming significant. When Re is small, the fountain starts to show the asymmetric behaviour at a much later time. For example, the $Re = 25$ fountain starts to become asymmetric in the X direction of the $Y - Z$ plane at $\tau \approx 450$ whereas when Re increases to 50, 100, and 200, the time for the onset of the asymmetric behaviour in this direction reduces to $\tau \approx 200$, 120, and 105, respectively. It is further observed that the magnitude of U_{max}/W_0 increases when Re increases, although the rate of increase decreases with Re . Similar behaviour is observed in the Y direction of the $Y - Z$ plane, but the onset of the asymmetric behaviour in this direction occurs at a much later time

than that in the X direction for each corresponding case when Re is no more than 100. For higher Re cases, the onset of the asymmetric behaviour in the Y direction occurs at essentially the same time as that in the X direction for each corresponding case. A quantitative analysis on the time for the onset of the asymmetric behavior (also termed the asymmetric transition time) in both the X and Y directions of the $Y - Z$ plane will be presented in Section 3.2.

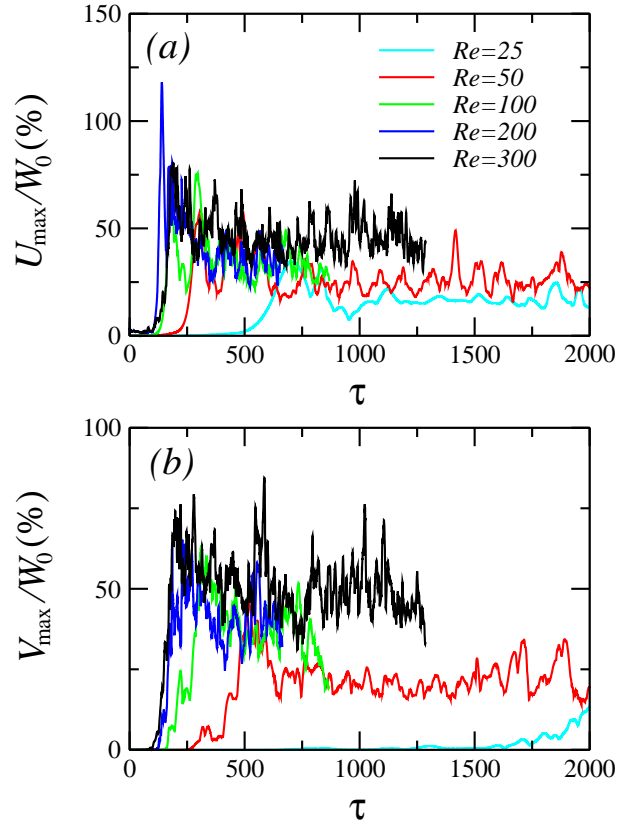


Figure 7: Time series of (a) U_{max}/W_0 and (b) V_{max}/W_0 for plane fountains at $X = 0$ in the $Y - Z$ plane with Re varying in the range $25 \leq Re \leq 300$ but all at $Fr = 10$ and $s = 0.1$.

3.1.3. Effect of s

Figure 8 presents the representative temperature contours at the quasi-steady **stage** on the same three individual planes as those in Fig. 5 when s varies in the range $0 \leq s \leq 0.5$, with Fr and Re kept constant at $Fr = 10$ and $Re = 100$. The results with $s = 0$, which represents the case with a homogeneous ambient fluid, are also included for comparison. Again all these plane fountains become asymmetric and unsteady, although the extent

of asymmetry and unsteadiness decreases with increasing s . It is also observed that the fountain height, as shown by the contours in the $X - Z$ plane, decreases when s increases, due to the increasing negative buoyancy that the fountain fluid has to overcome to penetrate in the linearly-stratified ambient fluid. In the $Y - Z$ plane, the increase in s leads to a lower fountain height and a smaller extent of the fluctuation of the height along the Y direction. Similarly, the increase in s leads to **a smaller extent of the fluctuation of the width in the $X - Y$ plane as well**. All these clearly demonstrate that the stratification of the ambient fluid plays a positive role to stabilize the flow and to alleviate its asymmetric and unsteady behavior.

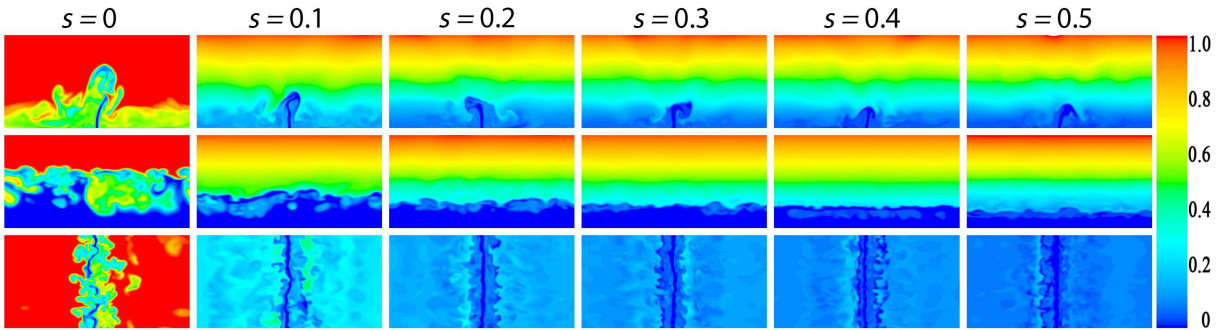


Figure 8: Representative temperature contours of plane fountains at the quasi-steady **stage** for different s values in the range $0 \leq s \leq 0.5$, all at $Fr = 10$ and $Re = 100$, at $Y = 0$ in the $X - Z$ plane (top row), $X = 0$ in the $Y - Z$ plane (middle row), and $Z = 0.5Z_{m,i}$ in the $X - Y$ plane (bottom row), respectively.

Figure 9 presents the corresponding representative contours of U/W_0 and V/W_0 at the quasi-steady stage at $X = 0$ in the $Y - Z$ plane for the same plane fountains as for Fig. 8. It is observed that significant non-zero U values are present at $X = 0$ in the $Y - Z$ plane at the quasi-steady **stage**, indicating that these fountains flap in the X direction in the $X - Z$ plane and become asymmetric and unsteady, which is in agreement with that observed from Fig. 8. However, due to the influence of the stratification to stabilize the flow and to reduce the asymmetric and unsteady behavior, as discussed above, it is observed that the extent of flapping and entrainment decreases when s increases, although the effect of s on the asymmetry and unsteadiness of the fountains is not as strong as that of Re . Similar observation can be made in the Y direction of the $Y - Z$ plane as well, although the magnitudes are smaller than those in the X direction.

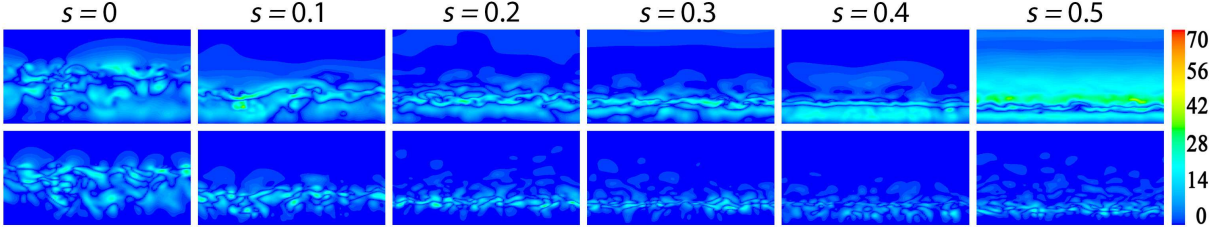


Figure 9: Representative contours of U/W_0 (top row) and V/W_0 (bottom row) of plane fountains at the quasi-steady state for different s values with $Fr = 10$ and $Re = 100$ at $X = 0$ in the $Y - Z$ plane, where U/W_0 and V/W_0 are in percentage.

Figure 10 presents the time series of U_{max}/W_0 and V_{max}/W_0 at $X = 0$ in the $Y - Z$ plane with s varying in the range $0.1 \leq s \leq 0.5$, all at $Fr = 10$ and $Re = 100$, which provides a better exhibition of the effect of s on the asymmetric behaviour of plane fountains in both the X and Y directions in the $Y - Z$ plane. For all s values considered, it is found that the fountains maintain symmetry in both directions at their respective early developing stages and become asymmetric and unsteady after that, which is in agreement with the above observation. Another noticeable observation is that the times for the onset of asymmetry in both directions do not change significantly when s varies, although it is evident that the onset of asymmetry in the Y direction occurs at a later time than that in the X direction for each corresponding case, as will be further analyzed quantitatively in the next section. A further observation is that the extent of asymmetry and unsteadiness in either direction, from a time-averaged perspective, is essentially the same for all s considered.

3.2. Quantitative analysis of the asymmetric transition time

3.2.1. In the X direction

To conduct a quantitative analysis of the time for the onset of the asymmetric behaviour of a plane fountain (i.e., the asymmetric transition time) in the X direction, which is denoted as $\tau_{asy,x}$, an appropriate threshold in terms of U_{max}/W_0 must be determined. To this end, $\tau_{asy,x}$ determined by the thresholds of $U_{max}/W_0 = 2\%$, 3% and 4% , respectively, are presented in Fig. 11 for varying s and Re . From this figure, it is seen that, for all three thresholds, $\tau_{asy,x}$ decreases when s increases, which is in agreement with the

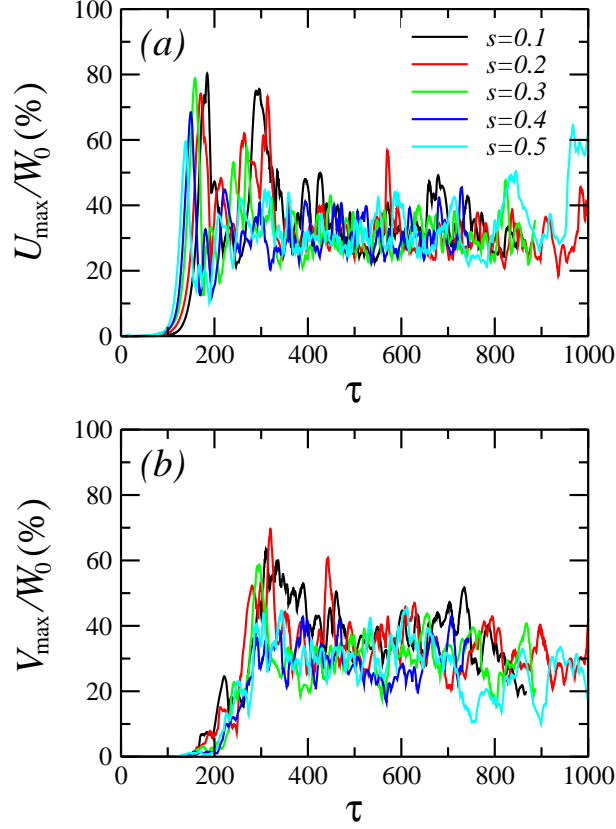


Figure 10: Time series of (a) U_{max}/W_0 and (b) V_{max}/W_0 for plane fountains at $X = 0$ in the $Y - Z$ plane with s varying in the range $0.1 \leq s \leq 0.5$ but all at $Fr = 10$ and $Re = 100$.

qualitative observations as described above, although $\tau_{asy,x}$ changes in a relatively narrow range (from about 100 to 135) when s varies in the range $0.1 \leq s \leq 0.5$. Similarly, it is observed that $\tau_{asy,x}$ decreases when Re increases, which is again in agreement with the above qualitative observations, but with a much wider range of changes (from about 530 to 100) when Re varies between 25 and 300. The figure also demonstrates that all three thresholds produce consistent results with similar trends and their differences are relatively small, in particular those between the thresholds with $U_{max}/W_0 = 3\%$ and 4% . Hence the threshold of $U_{max}/W_0 = 3\%$ is considered to be the appropriate threshold to determine $\tau_{asy,x}$ and is thus used in this study.

It is assumed that the effects of Re and s on $\tau_{asy,x}$ can be quantified by the following relation,

$$\tau_{asy,x} = C_{asy,x} Re^{-a} s^{-b}, \quad (12)$$

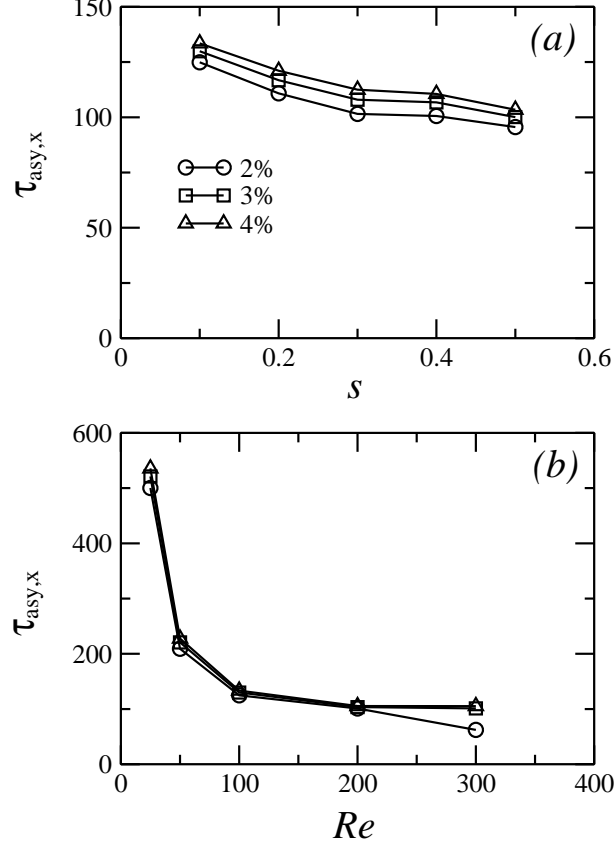


Figure 11: $\tau_{asy,x}$, determined by the thresholds of $U_{max}/W_0 = 2\%$, 3% and 4% , respectively, plotted against (a) s when $Fr = 10$ and $Re = 100$ and (b) Re when $Fr = 10$ and $s = 0.1$.

where $C_{asy,x}$ is the constant of proportionality and the indices a and b are constants which can be determined by a multivariable regression technique applied to the DNS results. Over the ranges $25 \leq Re \leq 300$ and $0.1 \leq s \leq 0.5$, the DNS results for the $Fr = 10$ plane fountains, as shown in Fig. 12(a), give the following quantified relations for $\tau_{asy,x}$ when the threshold of $U_{max}/W_0 = 3\%$ is used,

$$\tau_{asy,x} = 4064.1Re^{-0.731}s^{-0.189} - 42.1. \quad (13)$$

The regression coefficient of this correlation is 0.9362, indicating that this is a reasonably good relation. However, it is clearly seen from Fig. 12(a) that the DNS results at $Re = 25$ are significantly removed from the rest of the data, in terms of the relation (12). Such significant deviations at $Re = 25$ can also be seen in Fig. 11(b) where $\tau_{asy,x}$ drops dramatically when Re increases from 25 to 50. All these imply that the behavior of the

fountains at $Re = 25$, in terms of $\tau_{asy,x}$, is not in the same regime as the other fountains considered. This needs further study but is **not considered here**. It is also found that the datum for the case of $s = 0.5$ and $Re = 50$ is noticeably away from the rest of the data in terms of the relation (12) and thus should also be excluded. With the exclusion of this datum and all the data for $Re = 25$, the remaining DNS data presented in Fig. 12(a) are **found to be in very good** agreement with the relation (12), as shown in Fig. 12(b), which leads to the following quantified correlation,

$$\tau_{asy,x} = 632.5Re^{-0.433}s^{-0.252} - 3.8. \quad (14)$$

The regression coefficient of this correlation is 0.9711, confirming that this is a very good **fit**.

The noticeable deviation of the $Re = 50$ and $s = 0.5$ data from the quantified correlation is most likely due to the extremely large temperature gradient of the ambient fluid used in this DNS run, at $S = 212.4$ K/m as listed in Table 1, which is the largest among all DNS runs considered in this study. One consequence of the use of such an extremely large temperature gradient is that the **Oberbeck**-Boussinesq approximation assumed in the DNS run may not be appropriate. Furthermore, the use of such an extremely large temperature gradient for the $Re = 50$ and $s = 0.5$ case is found to lead to large deviations in other situations as well, as will be detailed subsequently in this paper.

As the index a for Re is significantly larger than the index b for s , the effect of Re on $\tau_{asy,x}$ is stronger than that of s , which confirms the qualitative observations as described above.

3.2.2. In the Y direction

Similarly, the asymmetric transition time in the Y direction, denoted as $\tau_{asy,y}$, also needs to be determined by using an appropriate threshold in terms of V_{max}/W_0 . Figure 13 presents $\tau_{asy,y}$, **determined** by different V_{max}/W_0 thresholds for varying Re and s . However, unlike the $\tau_{asy,x}$ case, it is seen that the thresholds with $V_{max}/W_0 \geq 1\%$ lead to inconsistent and significantly different values of $\tau_{asy,y}$ for varying Re and s . But thresholds with V_{max}/W_0 **of no more than** 0.5% are found to produce consistent results with similar trends and slight differences. In particular, the numerical results presented in this figure demonstrate that the thresholds of $V_{max}/W_0 = 0.1\%$ and 0.2% produce almost

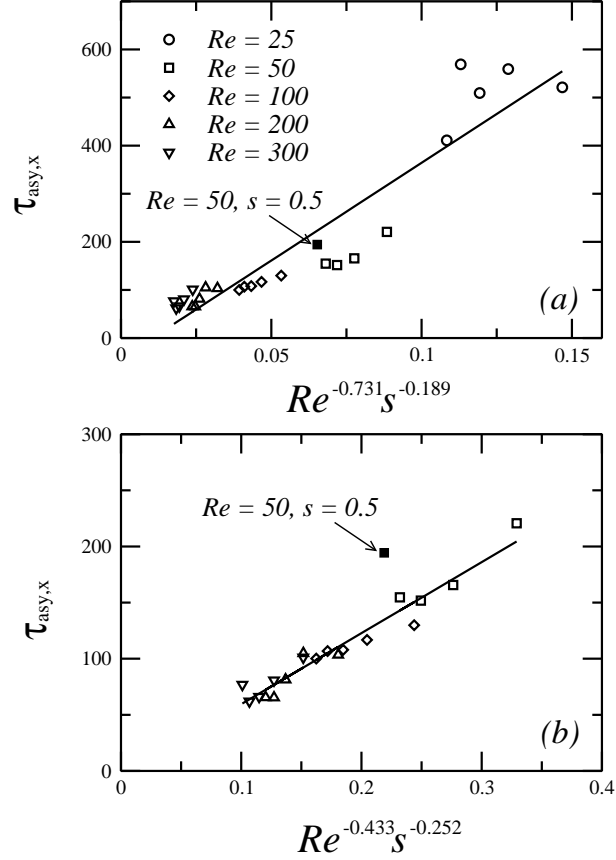


Figure 12: $\tau_{asy,x}$, determined with the $U_{max}/W_0 = 3\%$ threshold, plotted against (a) $Re^{-0.731}s^{-0.189}$ over the ranges $25 \leq Re \leq 300$ and $0.1 \leq s \leq 0.5$ and (b) $Re^{-0.433}s^{-0.252}$ over the ranges $50 \leq Re \leq 300$ and $0.1 \leq s \leq 0.5$. The solid lines are the linear fits of the data, with the $s = 0.5$ and $Re = 50$ datum excluded in (b).

identical values of $\tau_{asy,y}$. Hence, the threshold of $V_{max}/W_0 = 0.2\%$ is considered to be the appropriate threshold to determine $\tau_{asy,y}$ and is thus used in this study.

Similar to $\tau_{asy,x}$, the effects of Re and s on $\tau_{asy,y}$ is assumed to be quantified by the following relation,

$$\tau_{asy,y} = C_{asy,y} Re^{-c} s^{-d}, \quad (15)$$

where again the indices c and d and the constant of proportionality $C_{asy,y}$ are constants which are determined by applying the multivariable regression technique to the DNS results. With the DNS results for $\tau_{asy,y}$, over the ranges $25 \leq Re \leq 300$ and $0.1 \leq s \leq 0.5$, as shown in Fig. 14(a), the following quantified relation is obtained for $\tau_{asy,y}$ with the

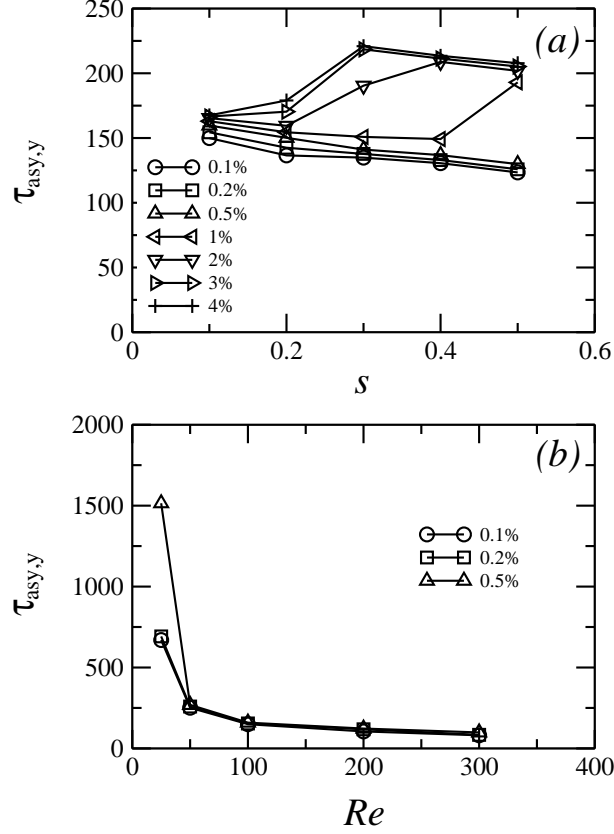


Figure 13: (a) $\tau_{asy,y}$, determined by the thresholds of $V_{max}/W_0 = 0.1\%$, 0.2% , 0.5% , 1% , 2% , 3% , and 4% , respectively, plotted against s when $Fr = 10$ and $Re = 100$, and (b) $\tau_{asy,y}$, determined by the thresholds of $V_{max}/W_0 = 0.1\%$, 0.2% , and 0.5% , respectively, plotted against Re when $Fr = 10$ and $s = 0.1$.

threshold of $V_{max}/W_0 = 0.2\%$,

$$\tau_{asy,y} = 34038.0Re^{-0.992}s^{-0.027} - 154.1. \quad (16)$$

From Fig. 14(a), it is apparent that the DNS results are not in good agreement with the relation (15), which is also confirmed by the low regression coefficient, at $R = 0.7964$, for the above quantified correlation. Similar to that for $\tau_{asy,x}$, the behavior of the fountains at $Re = 25$, in terms of $\tau_{asy,y}$, is also in a different regime from that of the other fountains considered, and thus should be excluded from the regression. **Furthermore**, the DNS datum for the case of $Re = 50$ and $s = 0.5$ should also be excluded from the regression for the **same reason as that for $\tau_{asy,x}$** , as discussed above. With the exclusion of this datum and all the data at $Re = 25$, the remaining DNS data presented in Fig. 14(a) are found

in very good agreement with the relation (15), as shown in Fig. 14(b), which leads to the following quantified correlation,

$$\tau_{asy,y} = 1533.2Re^{-0.542}s^{-0.129} - 4.2. \quad (17)$$

The regression coefficient of this correlation is 0.9904, confirming that this is a very good fit.

As the index c for Re is more than three times larger than the index d for s , the effect of Re on $\tau_{asy,y}$ is much stronger than that of s . A comparison of the values of a , b , c and d in the quantified relations (14) and (17) further shows that the effect of Re on $\tau_{asy,y}$ is also stronger than on $\tau_{asy,x}$, whereas on the contrary the effect of s on $\tau_{asy,y}$ is much weaker than on $\tau_{asy,x}$. All these are consistent with the qualitative observations as described above.

4. Maximum fountain height

4.1. Time series of the maximum fountain height

A typical time series of the dimensionless maximum fountain height, z_m ($z_m = Z_m/X_0$, where Z_m is the maximum fountain height), obtained from DNS, is presented as an example in Fig. 15 for the case of $Fr = 10$, $Re = 300$ and $s = 0.2$. It is seen that initially the fountain rises continuously after initiation until at $\tau_{m,i}$ when it attains an initial maximum height $z_{m,i}$. After that, z_m falls slightly before it rises again, followed by a short period of transition before it becomes fully developed subsequently, with z_m fluctuating around an almost constant value, $z_{m,a}$, which is denoted as the time-averaged maximum fountain height. $\tau_{m,i}$ (the time for the fountain to attain the initial maximum height $z_{m,i}$), $z_{m,i}$, $z_{m,a}$, σ which is the standard deviation of z_m around $z_{m,a}$ at the fully developed stage (the quasi-steady state), and the time period used for determining $z_{m,a}$ are illustrated in Fig. 15.

The DNS results for the time series of z_m for fountains with s and Re varying over the ranges $0.1 \leq s \leq 0.5$ and $25 \leq Re \leq 300$, all at $Fr = 10$, are presented in Fig. 16. It is observed that in general z_m decreases when s increases due to the increasing negative buoyancy, but increases when Re increases, largely due to the increased mixing and entrainment effects. It is also observed that $\tau_{m,i}$ reduces when s increases, again due to the

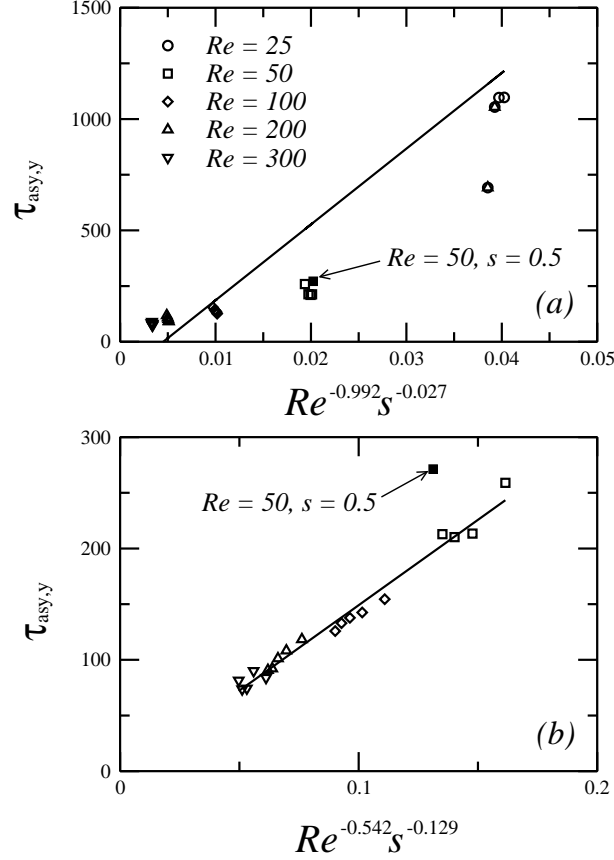


Figure 14: $\tau_{asy,y}$, determined with the $V_{max}/W_0 = 0.2\%$ threshold, plotted against (a) $Re^{-0.992}s^{-0.027}$ over the ranges $25 \leq Re \leq 300$ and $0.1 \leq s \leq 0.5$ and (b) $Re^{-0.532}s^{-0.129}$ over the ranges $50 \leq Re \leq 300$ and $0.1 \leq s \leq 0.5$. The solid lines are the linear fits of the data, with the $s = 0.5$ and $Re = 50$ datum excluded in (b).

increasing negative buoyancy which results in reduced z_m . $\tau_{m,i}$ is also observed to reduce when Re increases.

4.2. Initial maximum fountain height

4.2.1. Effect of Re

The effect of Re on $z_{m,i}$ is demonstrated by the DNS results presented in Fig. 17 for fountains over the ranges $25 \leq Re \leq 300$ and $0.1 \leq s \leq 0.5$. It is seen that when $Re \leq 100$, $z_{m,i}$ increases when Re increases. However, the dependence of $z_{m,i}$ on Re when $Re > 100$ is not monotonic and is strongly s dependent. For $s = 0.1$, $z_{m,i}$ continues to increase when Re increases, but for $s = 0.2$, it reduces at $Re = 200$ but increases again

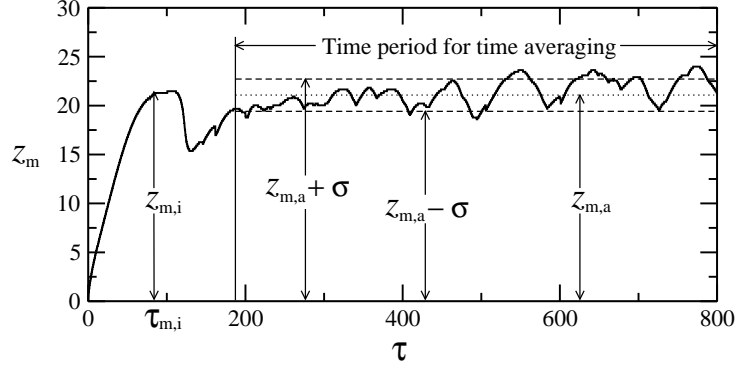


Figure 15: Illustration of $z_{m,i}$, $\tau_{m,i}$, $z_{m,a}$ and σ based on the time series of the dimensionless maximum fountain height, z_m , obtained from DNS for the case of $Fr = 10$, $Re = 300$ and $s = 0.2$. σ is the standard deviation of z_m around $z_{m,a}$ at the fully developed stage (*i.e.*, quasi-steady state).

when $Re = 300$, and for $s = 0.3$ it continues to reduce when Re increases, whereas for $s = 0.4$ and 0.5 , $z_{m,i}$ is almost constant for $Re \geq 100$. This implies that the fountain behavior, in terms of $z_{m,i}$, may be in different regimes when $Re \leq 100$ and when $Re \geq 100$. It is also observed that the dependence of $z_{m,i}$ on Re is in general not linear.

It is assumed that the dependence of $z_{m,i}$ on Re can be represented by the following relation,

$$z_{m,i} = C_{m,i,Re} Re^a, \quad (18)$$

where $C_{m,i,Re}$ is a constant of proportionality and the index a is also a constant. The regression results with this relation using the DNS data presented in Fig. 17(a), as demonstrated in Figs. 17(b) and 17(c) for $25 \leq Re \leq 300$ and $25 \leq Re \leq 100$, respectively, are listed in Table 2. It is found that over the range of $25 \leq Re \leq 300$, only the data with $s = 0.1$ agrees well with the relation (18), and at other s values, no very satisfactory agreement can be obtained. However, over the range of $25 \leq Re \leq 100$, the dependence of $z_{m,i}$ on Re is well predicted by the relation (18).

4.2.2. Effect of s

The effect of s on $z_{m,i}$ is shown in Fig. 18 for the fountains over the ranges $25 \leq Re \leq 300$ and $0.1 \leq s \leq 0.5$. In contrast to the effect of Re , it is seen from Fig. 18(a) that $z_{m,i}$ decreases monotonically with increasing s , which is the result of the increasing negative buoyancy that the fountains have to overcome when penetrating the stratified ambient

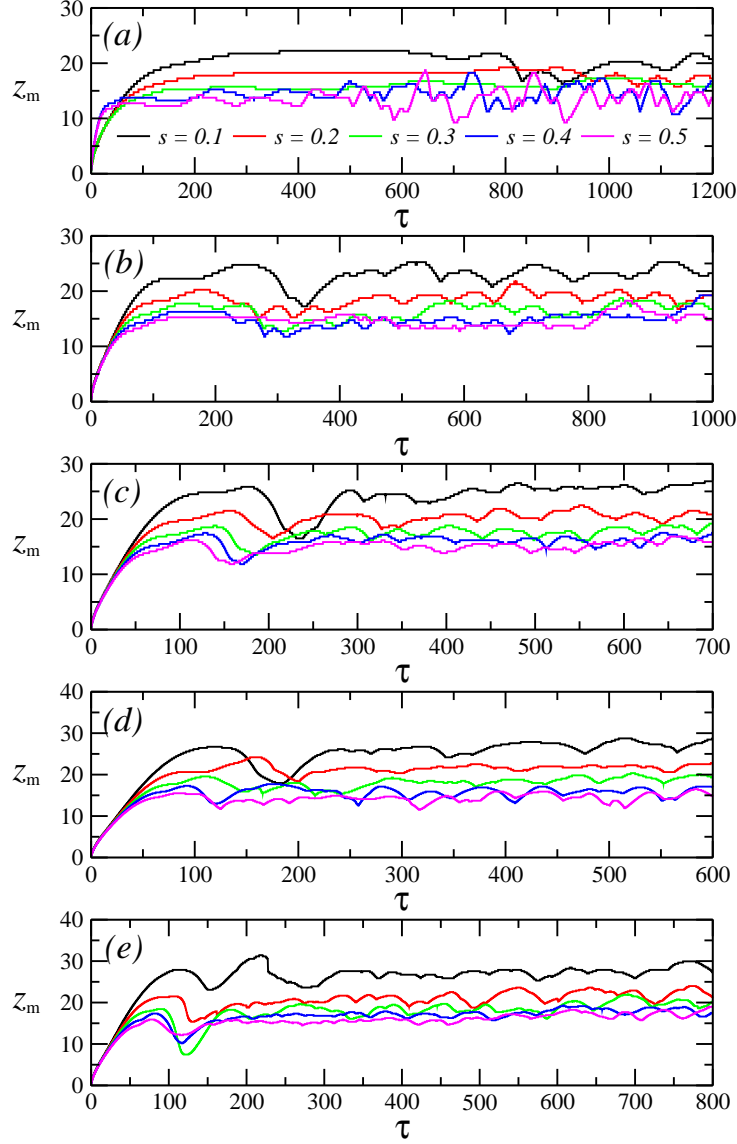


Figure 16: Time series of the maximum fountains height (z_m) within the whole computational domain for different value of s in the range $0.1 \leq s \leq 0.5$ at (a) $Re = 25$, (b) $Re = 50$, (c) $Re = 100$, (d) $Re = 200$, and (e) $Re = 300$, respectively, all at $Fr = 10$.

fluid. Similarly, the dependence of $z_{m,i}$ on s is in general not linear, and the DNS results presented in Fig. 18(b) clearly demonstrate that this dependence can be expressed by the following relation,

$$z_{m,i} = C_{m,i,s} s^b, \quad (19)$$

where $C_{m,i,s}$ is a constant of proportionality and the index b is also a constant. The regression results are listed in Table 3. It is found that over the ranges $25 \leq Re \leq 300$

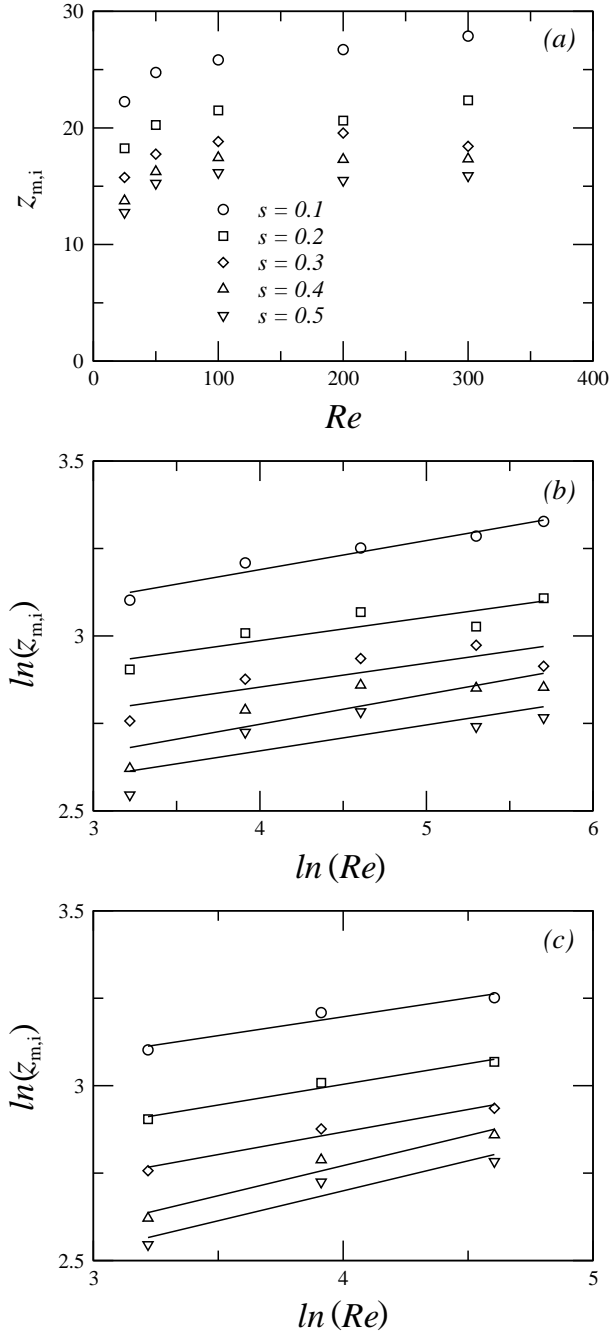


Figure 17: (a) $z_{m,i}$ plotted against Re and (b) $\ln(z_{m,i})$ plotted against $\ln(Re)$ for $25 \leq Re \leq 300$ and $0.1 \leq s \leq 0.5$, and (c) $\ln(z_{m,i})$ plotted against $\ln(Re)$ for $25 \leq Re \leq 100$ and $0.1 \leq s \leq 0.5$, all at $Fr = 10$. The solid lines are linear fit lines.

and $0.1 \leq s \leq 0.5$, all data agree very well with the relation (19), indicating that the dependence of $z_{m,i}$ on s is well represented by this relation.

Table 2: Regression results for the dependence of $z_{m,i}$ on Re for $25 \leq Re \leq 300$ and $25 \leq Re \leq 100$, respectively.

| s | For $25 \leq Re \leq 300$ | | | For $25 \leq Re \leq 100$ | | |
|-----|---------------------------|-------|--------|---------------------------|-------|--------|
| | $C_{m,i,Re}$ | a | R | $C_{m,i,Re}$ | a | R |
| 0.1 | 17.409 | 0.083 | 0.9744 | 15.904 | 0.108 | 0.9709 |
| 0.2 | 15.191 | 0.067 | 0.8738 | 12.566 | 0.118 | 0.9882 |
| 0.3 | 13.208 | 0.068 | 0.8306 | 10.509 | 0.129 | 0.9814 |
| 0.4 | 11.082 | 0.086 | 0.8528 | 8.034 | 0.172 | 0.9741 |
| 0.5 | 10.753 | 0.074 | 0.7803 | 7.492 | 0.171 | 0.9597 |

Table 3: Regression results for the dependence of $z_{m,i}$ on s for $25 \leq Re \leq 300$ and $0.1 \leq s \leq 0.5$.

| Re | $C_{m,i,s}$ | b | R |
|------|-------------|--------|--------|
| 25 | 10.124 | -0.350 | 0.9955 |
| 50 | 12.344 | -0.303 | 0.9998 |
| 100 | 13.328 | -0.290 | 0.9990 |
| 200 | 12.742 | -0.320 | 0.9886 |
| 300 | 12.419 | -0.353 | 0.9963 |

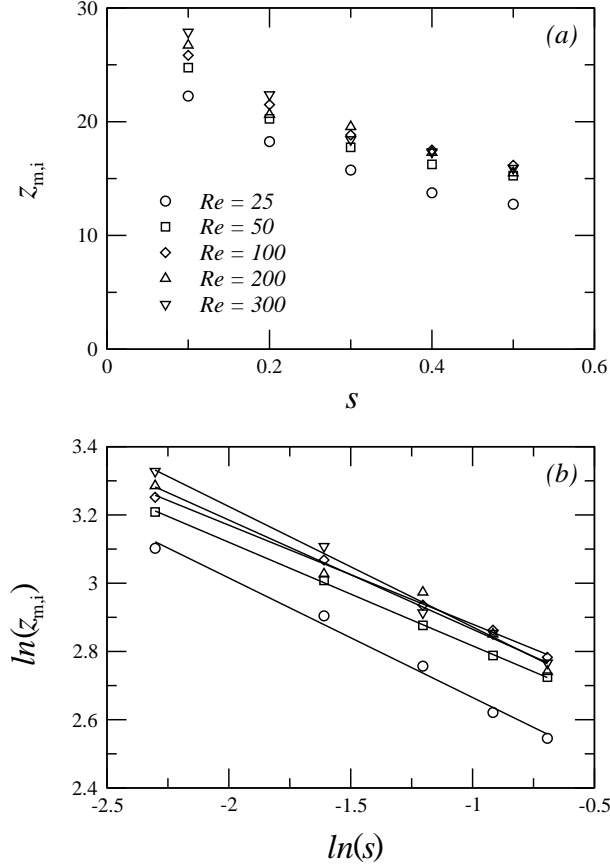


Figure 18: (a) $z_{m,i}$ plotted against s and (b) $\ln(z_{m,i})$ plotted against $\ln(s)$ for $25 \leq Re \leq 300$ and $0.1 \leq s \leq 0.5$, all at $Fr = 10$. The solid lines are linear fit lines.

4.2.3. Combined effect of Re and s

As the dependences of $z_{m,i}$ on Re and s are represented by the relations (18) and (19), respectively, the combined effect of Re and s on $z_{m,i}$ can be quantified by the following relation,

$$z_{m,i} = C_{m,i} Re^a s^b, \quad (20)$$

where $C_{m,i}$ is a constant of proportionality and the indices a and b are again constants. The values of these constants are determined by the multivariable regression method using the DNS results over the ranges of $25 \leq Re \leq 300$ and $0.1 \leq s \leq 0.5$, which gives the following quantified correlation,

$$z_{m,i} = 8.527 Re^{0.076} s^{-0.323} + 0.200. \quad (21)$$

The regression coefficient of this correlation is $R = 0.9835$, indicating that the DNS results over the ranges of $25 \leq Re \leq 300$ and $0.1 \leq s \leq 0.5$ are in very good agreement with the relation (20), as demonstrated in Fig. 19(a) where the DNS results for $z_{m,i}$ over the ranges of $25 \leq Re \leq 300$ and $0.1 \leq s \leq 0.5$ are plotted against $Re^{0.076}s^{-0.323}$. In view of the not very satisfactory agreement between the DNS results over the whole range of $25 \leq Re \leq 300$ with the relation (18), as described above, **this is a surprising** outcome. Nevertheless, this is the result of the much weaker dependence of $z_{m,i}$ on Re than on s , as the magnitude of b for s is more than three times larger than that of a for Re , as shown by the quantified correlation (21), and hence the contribution from Re to $z_{m,i}$ is significantly weakened in the combined effect of Re and s and the contribution from s is dominant.

There is no doubt that the separation of the range of Re , into **the ranges** $25 \leq Re \leq 100$ and $200 \leq Re \leq 300$ respectively, will further improve the agreement between the DNS results and the relation (20). Nevertheless, the improvements are found to be marginal, as shown in Fig. 19(b) for the range of $25 \leq Re \leq 100$ and Fig. 19(c) for the range of $200 \leq Re \leq 300$. The regression analysis gives

$$z_{m,i} = 6.673Re^{0.140}s^{-0.315} + 0.490, \quad (22)$$

for the range of $25 \leq Re \leq 100$, and

$$z_{m,i} = 9.828Re^{0.044}s^{-0.336} + 0.021, \quad (23)$$

for the range of $200 \leq Re \leq 300$. The regression coefficients for these two quantified correlations are 0.9922 and 0.9925, respectively, which confirm that the improvements are indeed very marginal. These results further show that the effect of Re on $z_{m,i}$ is significantly weakened when Re is large, with the value of a for the range of $200 \leq Re \leq 300$ less than one third of that for the range $25 \leq Re \leq 100$. It is expected that a further increase of Re , beyond $Re = 300$, will further weaken the effect of Re , and ultimately $z_{m,i}$ will be independent of Re when Re is sufficiently high. In fact, even for the range of $200 \leq Re \leq 300$, as shown in Fig. 19(d), the complete elimination of Re from the relation (20) is found to only very marginally weaken the agreement between the DNS results and the reduced relation (20), *i.e.*,

$$z_{m,i} = 12.583s^{-0.336} + 0.013, \quad (24)$$

with the regression coefficient of 0.9906, which is only very slightly lower than 0.9925 for the relation (23).

A further observation from Fig. 19 is that the value of b in the relation (20) barely changed when Re is in different regimes or no Re is included at all. This further demonstrates that in the combined effect of Re and s on $z_{m,i}$, the contribution from s is dominant.

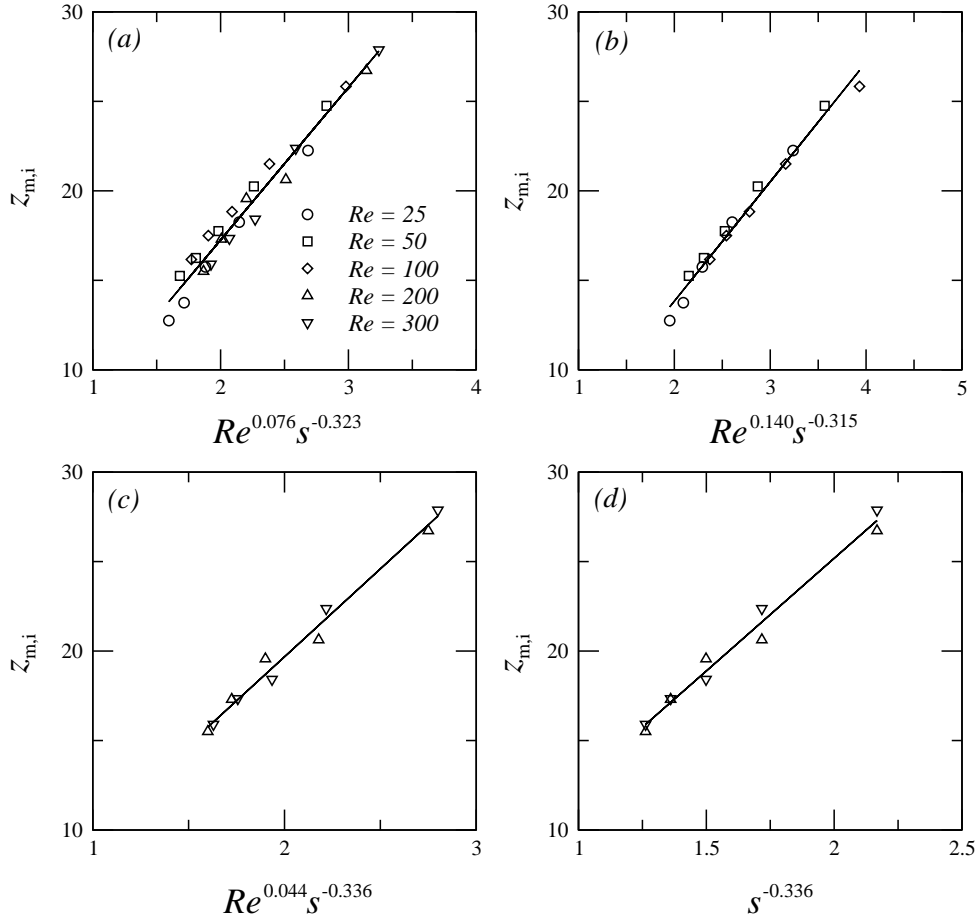


Figure 19: (a) $z_{m,i}$ plotted against $Re^{0.076} s^{-0.323}$ over the ranges of $25 \leq Re \leq 300$ and $0.1 \leq s \leq 0.5$, (b) $z_{m,i}$ plotted against $Re^{0.140} s^{-0.315}$ over the ranges of $25 \leq Re \leq 100$ and $0.1 \leq s \leq 0.5$, (c) $z_{m,i}$ plotted against $Re^{0.044} s^{-0.336}$ over the ranges of $200 \leq Re \leq 300$ and $0.1 \leq s \leq 0.5$, and (d) $z_{m,i}$ plotted against $s^{-0.336}$ over the ranges of $200 \leq Re \leq 300$ and $0.1 \leq s \leq 0.5$, respectively, all at $Fr = 10$. The solid lines are linear fit lines.

4.3. Time to reach the initial maximum fountain height

The effects of s and Re on the time to reach the initial maximum fountain height, $\tau_{m,i}$, which is made dimensionless by X_0/W_0 , are shown in Fig. 20 over the ranges $0.1 \leq s \leq 0.5$

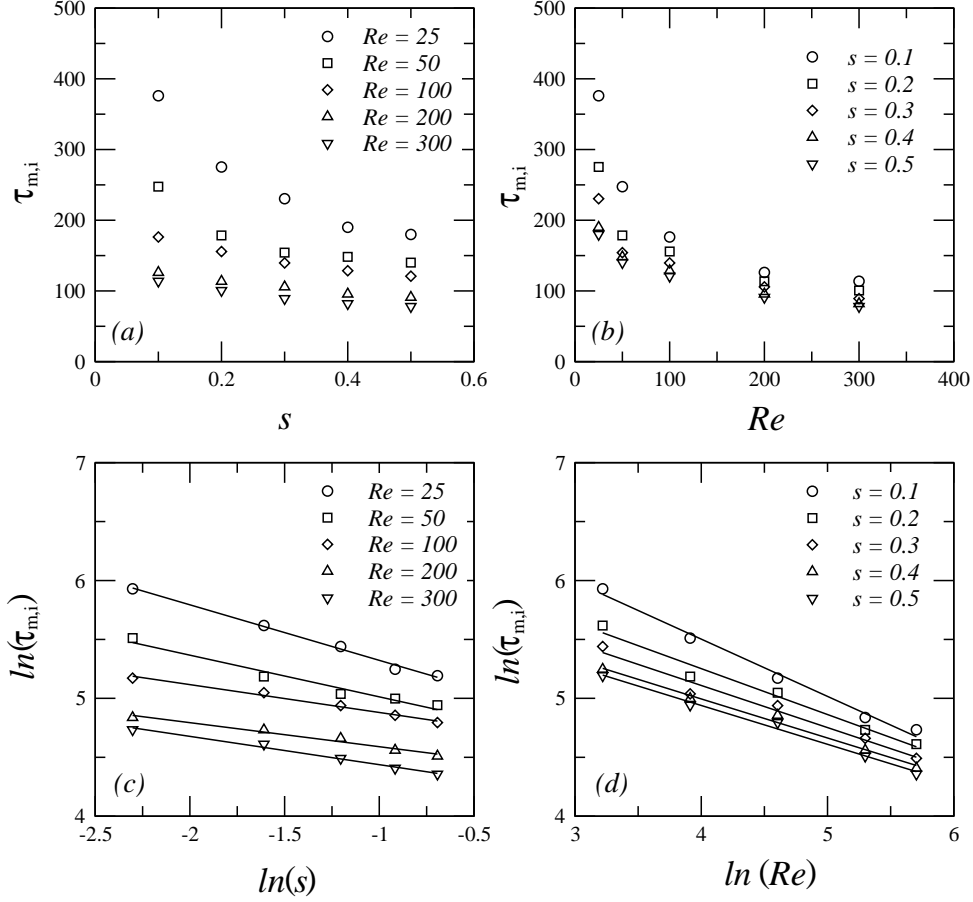


Figure 20: $\tau_{m,i}$ plotted against (a) s and (b) Re , and $\ln(\tau_{m,i})$ plotted against (c) $\ln(s)$ and (d) $\ln(Re)$, respectively, for the $Fr = 10$ fountains over the ranges of $25 \leq Re \leq 300$ and $0.1 \leq s \leq 0.5$. The solid lines are linear fit lines.

and $25 \leq Re \leq 300$. From Figs. 20(a) and 20(b) it is seen that in general $\tau_{m,i}$ decreases when s or Re increases, which is similar to that for the asymmetric transition time as discussed in § 3.2. The dependence of $\tau_{m,i}$ on s or Re is again not linear, and may be assumed to have the following relations,

$$\tau_{m,i} = C_{\tau,s} s^b, \quad (25)$$

and

$$\tau_{m,i} = C_{\tau,Re} Re^a, \quad (26)$$

where $C_{\tau,s}$ and $C_{\tau,Re}$ are constants of proportionality, and the indices a and b are also constants. The regression analysis of the DNS results presented in Figs. 20(a) and 20(b)

Table 4: Regression results for the dependence of $\tau_{m,i}$ on s and Re respectively for $25 \leq Re \leq 300$ and $0.1 \leq s \leq 0.5$.

| Re | For $\tau_{m,i} = C_{\tau,s}s^b$ | | | For $\tau_{m,i} = C_{\tau,Re}Re^a$ | | | |
|------|----------------------------------|--------|--------|------------------------------------|---------------|--------|--------|
| | $C_{\tau,s}$ | b | R | s | $C_{\tau,Re}$ | a | R |
| 25 | 128.1 | -0.471 | 0.9971 | 0.1 | 1715.4 | -0.486 | 0.9950 |
| 50 | 105.6 | -0.354 | 0.9826 | 0.2 | 906.6 | -0.389 | 0.9874 |
| 100 | 104.0 | -0.236 | 0.9938 | 0.3 | 691.6 | -0.357 | 0.9853 |
| 200 | 80.3 | -0.204 | 0.9855 | 0.4 | 556.8 | -0.332 | 0.9943 |
| 300 | 66.5 | -0.240 | 0.9937 | 0.5 | 522.0 | -0.329 | 0.9954 |

with these two relations gives the values of $C_{\tau,s}$, $C_{\tau,Re}$, a and b as listed in Table 4. The DNS results are in very good agreement with the relations (25) and (26), as shown in Figs. 20(c) and 20(d). The results presented in Table 4 show that the magnitude of the index a , which represents the extent of the dependence of $\tau_{m,i}$ on s , generally decreases when Re increases, indicating that the dependence of $\tau_{m,i}$ on s becomes weakened when Re increases. Similarly, the magnitude of the index b , which represents the extent of the dependence of $\tau_{m,i}$ on Re , generally decreases when s increases, indicating that the dependence of $\tau_{m,i}$ on Re becomes weakened when s increases.

As the dependence of $\tau_{m,i}$ on Re and s is represented by the relations (25) and (26), respectively, the combined effect of Re and s on $\tau_{m,i}$ can be quantified by the following relation,

$$\tau_{m,i} = C_{\tau,i}Re^a s^b, \quad (27)$$

where $C_{\tau,i}$ is a constant of proportionality and the indices a and b are again constants. With all data over the ranges $25 \leq Re \leq 300$ and $0.1 \leq s \leq 0.5$, the regression analysis gives the values of -0.379 and -0.3 to a and b , respectively. However, as demonstrated in Fig. 21, the DNS results for $Re = 25$ and $s = 0.1$ and $s = 0.2$ are considerably removed from the other data in terms of the relation (27), most likely for a similar reason to that of the asymmetric transition time as discussed above (*i.e.*, the behavior at $Re = 25$ is in a different regime) and should be excluded in the regression. With the exclusion of the data at $Re = 25$ and $s = 0.1$ and $s = 0.2$, the regression analysis with the remaining DNS

results presented in Fig. 21 gives the following quantified correlation,

$$\tau_{m,i} = 493.2Re^{-0.379}s^{-0.3} + 7.101. \quad (28)$$

The regression coefficient of this correlation is $R = 0.9836$, confirming that this is a very good agreement.

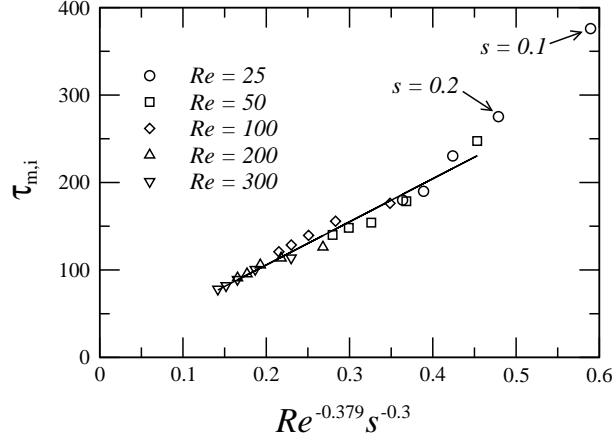


Figure 21: $\tau_{m,i}$ plotted against $Re^{-0.379}s^{-0.3}$ over the ranges $25 \leq Re \leq 300$ and $0.1 \leq s \leq 0.5$. The solid line is the linear fit of the data with the data at $Re = 25$ and $s = 0.1$ and $s = 0.2$ excluded.

4.4. Time-averaged maximum fountain height

4.4.1. Effect of Re

The effect of Re on $z_{m,a}$ is demonstrated by the DNS results presented in Fig. 22 for fountains over **the ranges** $25 \leq Re \leq 300$ and $0.1 \leq s \leq 0.5$, all at $Fr = 10$. From Fig. 22(a), it is observed that in general $z_{m,a}$ increases when Re increases for each s value, which is slightly different from that for $z_{m,i}$ in which the fountain behavior, in terms of $z_{m,i}$, may be in different regimes when $Re \leq 100$ and when $Re \geq 100$, as discussed above. The results also show that the dependence of $z_{m,a}$ on Re is in general not linear, and thus the following relation may be assumed,

$$z_{m,a} = C_{m,a,Re}Re^a, \quad (29)$$

where $C_{m,a,Re}$ is a constant of proportionality and the index a is again a constant. The regression results with this relation using the DNS data presented in Fig. 22(a), as demonstrated in Fig. 22(b), are listed in Table 5. It is found that over **the ranges** $25 \leq Re \leq 300$,

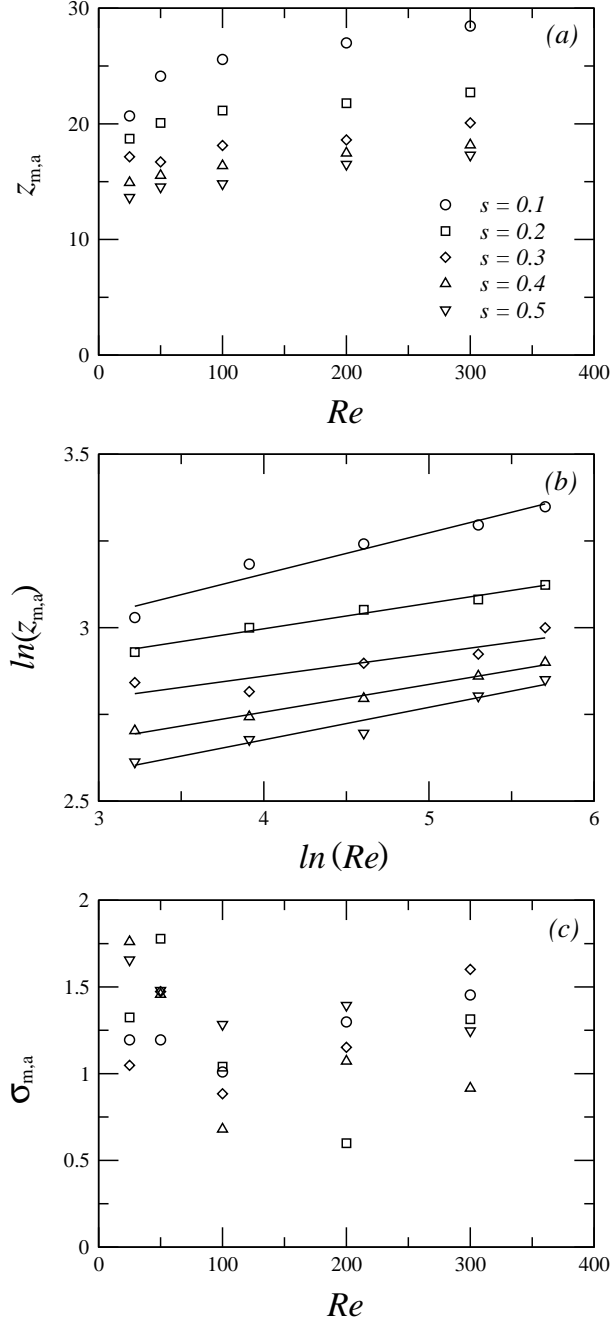


Figure 22: (a) $z_{m,a}$ plotted against Re , (b) $\ln(z_{m,a})$ plotted against $\ln(Re)$, and (c) $\sigma_{m,a}$ plotted against Re for $25 \leq Re \leq 300$ and $0.1 \leq s \leq 0.5$, all at $Fr = 10$. The solid lines are linear fit lines.

the data for each s value, except for $s = 0.3$, are in very good agreement with the relation (29). For $s = 0.3$, it is noted that the data at $Re = 50$ is noticeably removed from the quantified linear fit line. This is expected to have a similar cause to that discussed above

Table 5: Regression results for the dependence of $z_{m,a}$ on Re for $25 \leq Re \leq 300$ and $0.1 \leq s \leq 0.5$.

| s | $C_{m,a,Re}$ | a | R |
|-----|--------------|-------|--------|
| 0.1 | 14.579 | 0.119 | 0.9745 |
| 0.2 | 14.907 | 0.074 | 0.9907 |
| 0.3 | 13.480 | 0.065 | 0.9038 |
| 0.4 | 11.433 | 0.080 | 0.9953 |
| 0.5 | 9.996 | 0.094 | 0.9758 |

for $\tau_{asy,x}$ in the case of $s = 0.5$ and $Re = 50$, but a further investigation on this, which is beyond the scope of the current study, is needed. The DNS results for the time-averaged standard deviation of z_m around $z_{m,a}$ at the fully developed stage, $\sigma_{m,a}$, as illustrated in Fig. 15, are presented in Fig. 22(c). It is seen that over the ranges of $25 \leq Re \leq 300$ and $0.1 \leq s \leq 0.5$, $\sigma_{m,a}$ varies between 0.5 and 2.0, and has no noticeable dependence on either Re or s .

4.4.2. Effect of s

The effect of s on $z_{m,a}$ is shown in Fig. 23 for the fountains over **the ranges** $25 \leq Re \leq 300$ and $0.1 \leq s \leq 0.5$, all at $Fr = 10$. The DNS results presented in Fig. 23(a) show that $z_{m,a}$ decreases monotonically with increasing s , which is similar to that for $z_{m,i}$, as described above. This is again due to the increasing negative buoyancy that the fountains have to overcome when penetrating the stratified ambient fluid when s increases. Similarly, the dependence of $z_{m,a}$ on s is in general not linear, and the DNS results presented in Fig. 23(b) clearly demonstrate that this dependence can be expressed by the following relation,

$$z_{m,a} = C_{m,a,s} s^b, \quad (30)$$

where $C_{m,a,s}$ is a constant of proportionality and the index b is also a constant. The regression results are listed in Table 6. It is found that over **the ranges** $25 \leq Re \leq 300$ and $0.1 \leq s \leq 0.5$, all data agree very well with the relation (30), indicating that the dependence of $z_{m,a}$ on s is well represented by this relation. The DNS results for $\sigma_{m,a}$ are

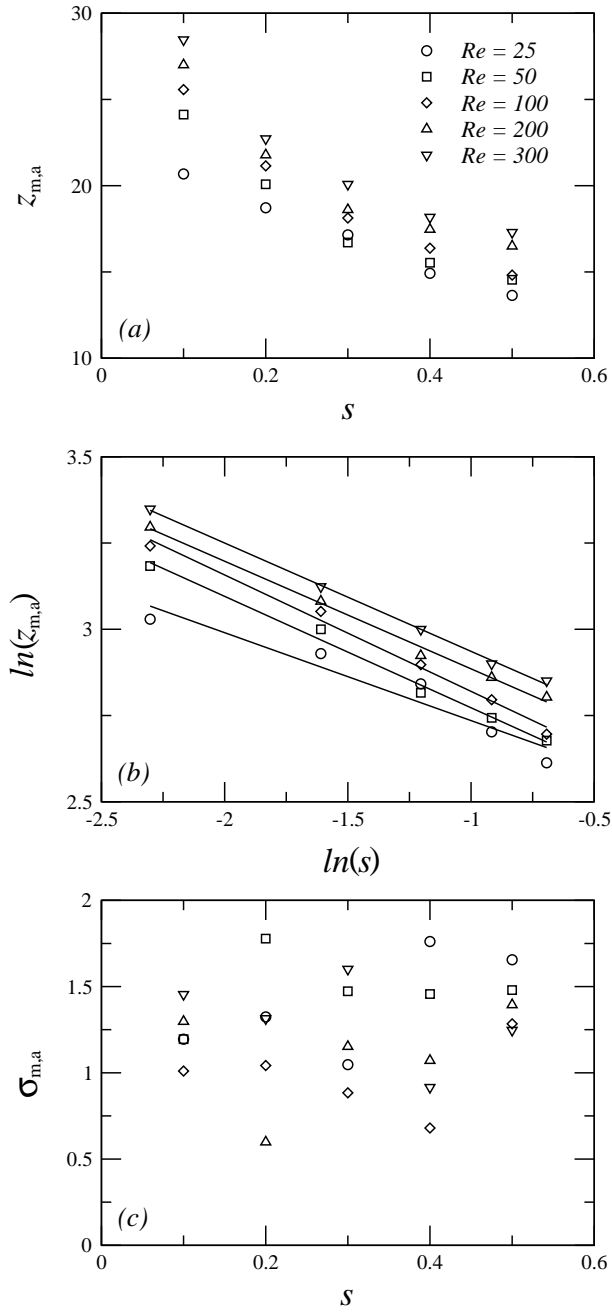


Figure 23: (a) $z_{m,a}$ plotted against s , (b) $\ln(z_{m,a})$ plotted against $\ln(s)$, and (c) $\sigma_{m,a}$ plotted against s for $25 \leq Re \leq 300$ and $0.1 \leq s \leq 0.5$, all at $Fr = 10$. The solid lines are linear fit lines.

presented in Fig. 23(c), which again demonstrate that $\sigma_{m,a}$ has no noticeable dependence on either Re or s .

Table 6: Regression results for the dependence of $z_{m,a}$ on s for $25 \leq Re \leq 300$ and $0.1 \leq s \leq 0.5$.

| Re | $C_{m,a,s}$ | b | R |
|------|-------------|-------|--------|
| 25 | 11.948 | 0.255 | 0.9638 |
| 50 | 11.581 | 0.323 | 0.9954 |
| 100 | 11.971 | 0.337 | 0.9959 |
| 200 | 13.110 | 0.312 | 0.9972 |
| 300 | 13.769 | 0.314 | 0.9992 |

4.4.3. Combined effect of Re and s

Similar to $z_{m,i}$, the combined effect of Re and s on $z_{m,a}$ can be quantified by the following relation,

$$z_{m,a} = C_{m,a} Re^a s^b, \quad (31)$$

where $C_{m,a}$ is a constant of proportionality and the indices a and b are again constants. With all data over **the ranges** $25 \leq Re \leq 300$ and $0.1 \leq s \leq 0.5$, the regression analysis gives the following quantified correlation,

$$z_{m,a} = 8.434 Re^{0.086} s^{-0.310} - 0.042. \quad (32)$$

The regression coefficient of this correlation is $R = 0.9902$, indicating that the DNS results over **the ranges** $25 \leq Re \leq 300$ and $0.1 \leq s \leq 0.5$ are in very good agreement with the relation (31), as illustrated in Fig. 24 where the DNS results for $z_{m,a}$ are plotted against $Re^{0.086} s^{-0.310}$. It is found that the values of the indices a and b , 0.086 and -0.310, are very close to those obtained for $z_{m,i}$ (0.076 and -0.323, respectively), which also demonstrates that the dependence of $z_{m,a}$ on Re is much weaker than that on s , again similar to $z_{m,i}$.

4.5. Variation of maximum fountain height at $X = 0$ on the $Y - Z$ plane

Before the onset of the asymmetric behavior, the maximum fountain height at $X = 0$ on the $Y - Z$ plane should be constant along the Y direction. However, after the onset of the asymmetric behavior, it is expected that the maximum fountain height on the $Y - Z$ plane will vary along the Y direction, as depicted in Fig. 25, where the Y -direction profile

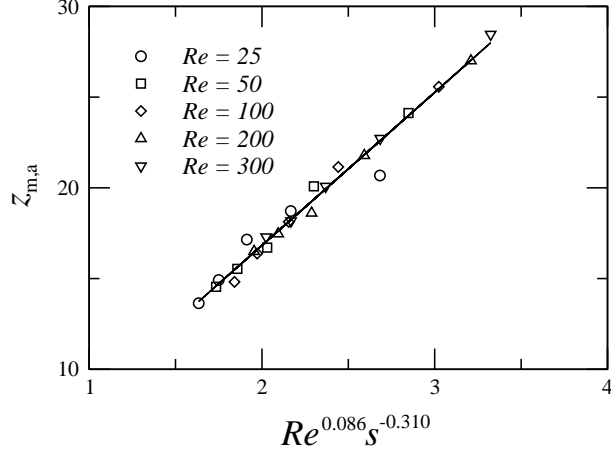


Figure 24: $z_{m,a}$ plotted against $Re^{0.086} s^{-0.310}$ over the ranges of $25 \leq Re \leq 300$ and $0.1 \leq s \leq 0.5$, all at $Fr = 10$. The solid line is a linear fit line.

of the maximum fountain height ($z_{x=0}$) at $X = 0$ on the $Y - Z$ plane, at time $\tau = 1072.4$, is presented for the case of $Re = 100$, $s = 0.2$, and $Fr = 10$. The parameter to quantify the variation of $z_{x=0}$ in the Y direction is the standard deviation of $z_{x=0}$ around its average in the Y direction, $z_{x=0,a}$, which is denoted as $\sigma_{x=0}$ and is made dimensionless by X_0 .

The time series of $\sigma_{x=0}$ for the $Fr = 10$ plane fountains over the ranges $25 \leq Re \leq 300$ and $0.1 \leq s \leq 0.5$, obtained by DNS, are presented in Fig. 26. The results show that for $25 \leq Re \leq 100$, in general the value of $\sigma_{x=0}$ increases when Re increases, and at $Re = 25$ the value is small, normally within 0.3, but dramatically increases to up to 4 when Re increases from 25 to 50. However, a further increase of Re , to beyond $Re = 100$, does not lead to a further increase in $\sigma_{x=0}$, as the results show that at $Re = 200$ and 300, the values of $\sigma_{x=0}$ are very close to those at $Re = 100$ for each s value. Another noticeable observation is that in general the values of $\sigma_{x=0}$ decrease when s increases, which is apparently due to the positive role of the stratification of the ambient fluid in stabilizing the flow and reducing the asymmetric and unsteady behavior of the fountains, as discussed above.

The dependence of $\sigma_{x=0}$ on s can be further demonstrated by the DNS results presented in Fig. 27 where $\sigma_{x=0,a}$, which is the time average of $\sigma_{x=0}$ over the period from the instant when $\sigma_{x=0}$ becomes significant to the end of the DNS run (which is essentially the fully developed stage), is plotted against s over the ranges of $25 \leq Re \leq 300$ and $0.1 \leq s \leq 0.5$.

It is seen that for each Re value, the data with different s values fall approximately on the same straight line, with a negative gradient, confirming that $\sigma_{x=0}$ decreases when s increases. The relation between $\sigma_{x=0,a}$ and s for each Re value can then be quantified by the following linear relation,

$$\sigma_{x=0,a} = c + ds, \quad (33)$$

where c and d are constants. The values of c and d are obtained by the regression analysis of the DNS results presented in Fig. 27 and the results are listed in Table 7. From these results, it is observed that in general the DNS results are in good agreement with the linear relation (33) for each Re value. It is further observed that the magnitudes of c and d for $Re = 25$ are significantly smaller than those for the other Re values, which further **indicates** that the behavior of the fountains at $Re = 25$ is in a different regime from the fountains at the other Re values considered. Again the datum at $Re = 50$ and $s = 0.5$ is considerably away from the other data in the trend, apparently due to the similar reason as discussed above for $\tau_{asy,x}$.

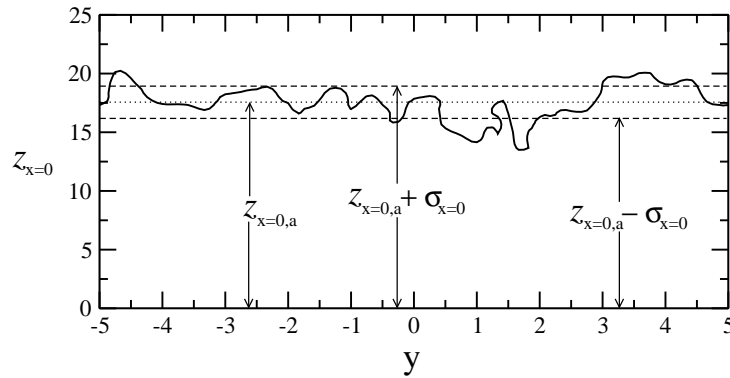


Figure 25: The DNS results for the Y -direction profile of the maximum fountain height $z_{x=0}$ at $X = 0$ on the $Y - Z$ plane at time $\tau = 1072.4$ for the case of $Re = 100$, $s = 0.2$, and $Fr = 10$, and the illustration of $z_{x=0,a}$, which is the average of $z_{x=0}$ along the Y direction, and the standard deviation $\sigma_{x=0}$ of $z_{x=0}$ around $z_{x=0,a}$ along the Y direction, where $y = Y/X_0$ is the dimensionless form of Y .

5. Conclusions

The three-dimensional DNS results for transitional plane fountains in linearly-stratified fluids with $25 \leq Re \leq 300$ and $0 \leq s \leq 0.5$, all at $Fr = 10$, have been used to analyze,

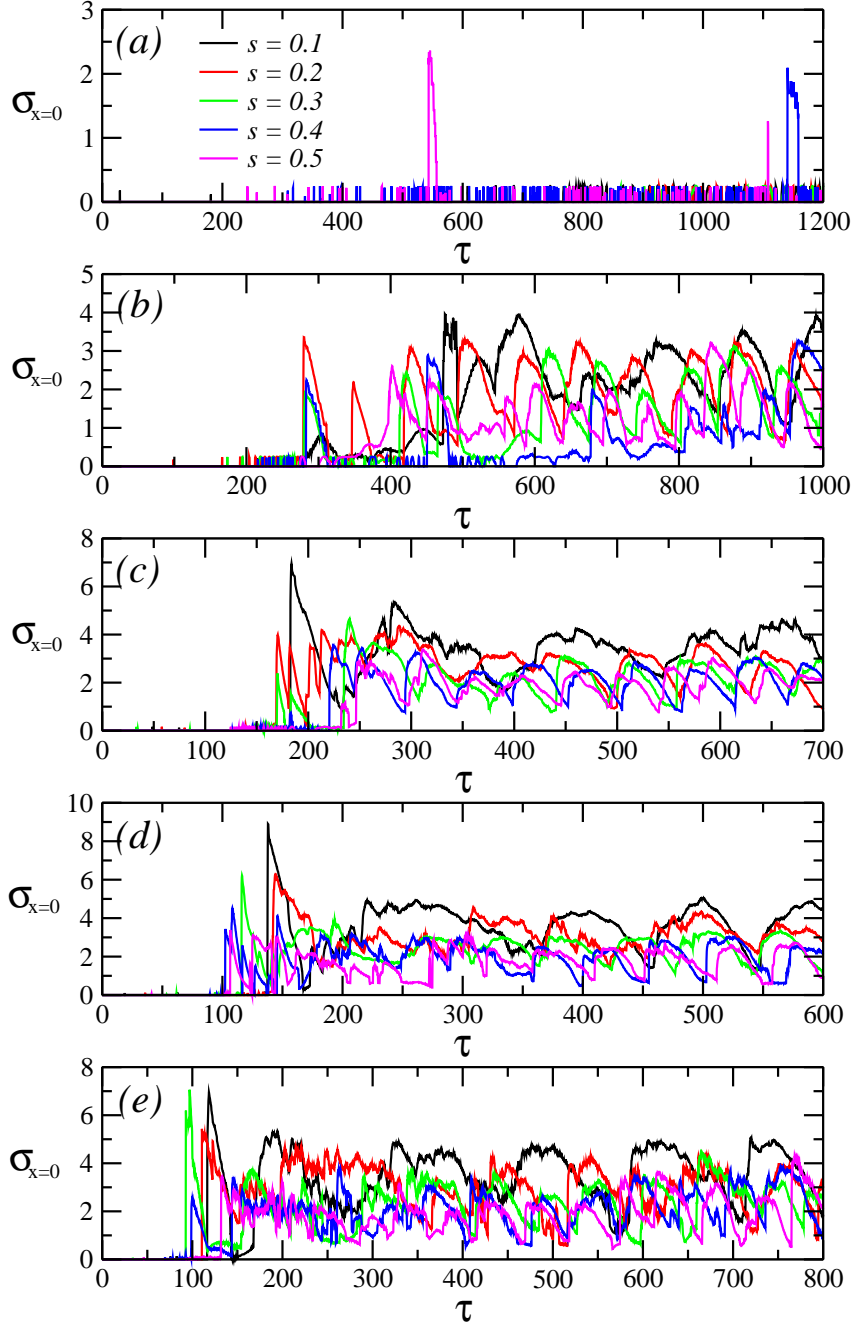


Figure 26: Time-series of $\sigma_{x=0}$ at $X = 0$ on the $Y - Z$ plane for the $Fr = 10$ fountains over the ranges of $25 \leq Re \leq 300$ and $0.1 \leq s \leq 0.5$: (a) $Re = 25$, (b) $Re = 50$, (c) $Re = 100$, (d) $Re = 200$, and (e) $Re = 300$.

both qualitatively and quantitatively, the transition of the fountains to asymmetry, their asymmetric behavior, and their maximum penetration heights.

It is found that over the ranges of Re and s considered, fountains are symmetric

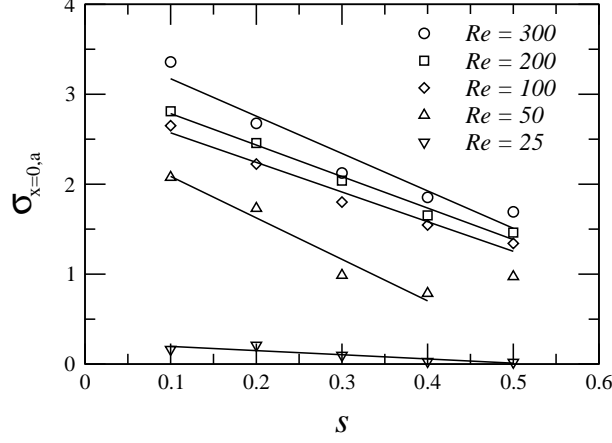


Figure 27: $\sigma_{x=0,a}$ plotted against s over the ranges $25 \leq Re \leq 300$ and $0.1 \leq s \leq 0.5$. The solid lines are linear fit lines.

Table 7: Regression results for the dependence of $\sigma_{x=0,a}$ on s for $25 \leq Re \leq 300$ and $0.1 \leq s \leq 0.5$.

| Re | c | d | R |
|------|-------|--------|-------|
| 25 | 0.255 | -0.490 | 0.891 |
| 50 | 2.637 | -4.702 | 0.982 |
| 100 | 3.035 | -3.379 | 0.985 |
| 200 | 3.258 | -3.678 | 0.993 |
| 300 | 3.676 | -4.217 | 0.964 |

in the early developing stage, but become asymmetric and unsteady after that. The fountains flap around $X = 0$ in the X - Z plane, with the fountain heights and the extent of entrainment increasing with Re . The increase of Re also leads to a larger fluctuation of the fountain height in the Y direction of the $Y - Z$ plane and a larger fountain width and increased fluctuation in the $X - Y$ plane. However, the stratification of the ambient fluid (*i.e.*, s) is shown to play a positive role in stabilizing the flow and reducing its asymmetric and unsteady behavior.

The results further demonstrate that the asymmetric behaviour of plane fountains in both the X and Y directions of the $Y - Z$ plane can be well represented by U_{max}/W_0 and V_{max}/W_0 at $X = 0$ of the plane, where U_{max} and V_{max} are the maximum values of U

and V at $X = 0$ in the $Y - Z$ plane, respectively. Any non-zero U_{max} or V_{max} indicates the asymmetric behaviour in the X or Y direction on the plane. It is found that the magnitude of U_{max}/W_0 increases when Re increases, although the rate of the increase decreases with Re . Similar behaviour is observed in the Y direction of the $Y - Z$ plane, but the onset of the asymmetric behaviour in this direction in general occurs at a much later time than that in the X direction. It is also observed that the extent of flapping and entrainment decreases when s increases, although the effect of s on the asymmetry and unsteadiness of the fountains is not as strong as that of Re . Empirical correlations which quantify the effects of Re and s are developed for the times for the onset of the asymmetric behaviour of plane fountains both in the X and Y directions, using the numerical results.

The numerical results further show that s has a stronger effect on $z_{m,i}$ and $z_{m,a}$ than Re does, but the dependence of $\tau_{m,i}$ on Re weakens when s increases, where $z_{m,i}$ and $z_{m,a}$ are the initial and time-averaged maximum fountain heights, and $\tau_{m,i}$ is the time to attain the initial maximum fountain height. Empirical correlations are developed to quantify the individual and combined effects of Re and s on these three parameters.

The numerical results also demonstrate that the behavior of the plane fountains at $Re = 25$ is not in the same regime as the other fountains considered, which needs further investigation but is beyond the scope of the current study.

Acknowledgment

The authors would like to thank the anonymous reviewers for their constructive comments and suggestions. The support from the National Natural Science Foundation of China (51469035, 51266016) and the Australian Research Council (ARC) is gratefully acknowledged. M. I. Inam also thanks James Cook University for the JCUPRS scholarship.

References

- [1] B.R. Morton, Forced plumes, *J. Fluid Mech.* 5 (1959) 151–163.
- [2] N. Williamson, S.W. Armfield, W. Lin, Transition behavior of weak turbulent fountains, *J. Fluid Mech.* 655 (2010) 306–326.

- [3] N. Srinarayana, N. Williamson, S.W. Armfield, W. Lin, Line fountain behavior at low-Reynolds number, *Int. J. Heat Mass Transfer* 53 (2010) 2065–2073.
- [4] O.J. Myrtroeen, G.R. Hunt, Negatively buoyant projectiles – from weak fountains to heavy vortices, *J. Fluid Mech.* 657 (2010) 227–237.
- [5] G. Carazzo, E. Kaminski, S. Tait, The rise and fall of turbulent fountains: a new model for improved quantitative predictions, *J. Fluid Mech.* 657 (2010) 265–284.
- [6] N. Williamson, S. W. Armfield, W. Lin, Forced turbulent fountain flow behaviour, *J. Fluid Mech.* 671 (2011) 535–558.
- [7] H.C. Burridge, G.R. Hunt, The rise heights of low- and high-Froude-number turbulent axisymmetric fountains, *J. Fluid Mech.* 691 (2012) 392–416.
- [8] H.C. Burridge, G.R. Hunt, The rhythm of fountains: the length and time scales of rise height fluctuations at low and high Froude number fountains, *J. Fluid Mech.* 728 (2013) 91–119.
- [9] N. Srinarayana, S.W. Armfield, W. Lin, Behaviour of laminar plane fountains with a parabolic inlet velocity profile in a homogeneous fluid, *Int. J. Thermal Sci.* 67 (2013) 87–95.
- [10] H.C. Burridge, G.R. Hunt, Scaling arguments for the fluxes in turbulent miscible fountains, *J. Fluid Mech.* 744 (2014) 273–285.
- [11] B.R. Vinoth, P.K. Panigrahi, Characteristics of low Reynolds number non-Boussinesq fountains from non-circular sources, *Phys. Fluids* 26 (2014) 014106.
- [12] A.B. Shrinivas, G.R. Hunt, Unconfined turbulent entrainment across density interfaces, *J. Fluid Mech.* 757 (2014) 573–598.
- [13] N.B. Kaye, G.R. Hunt, Weak fountains, *J. Fluid Mech.* 558 (2006) 319–328.
- [14] W. Lin, S.W. Armfield, Onset of entrainment in transitional round fountains, *Int. J. Heat Mass Transfer* 51 (2008) 5226–5237.

- [15] N. Williamson, N. Srinarayana, S.W. Armfield, G.D. McBain, W. Lin, Low-reynolds-number fountain behaviour, *J. Fluid Mech.* 608 (2008) 297–318.
- [16] G.R. Hunt, H.C. Burridge, Fountains in industry and nature, *Annu. Rev. Fluid Mech.* 47 (2015) 195–220.
- [17] J.S. Turner, Jets and plumes with negative or reversing buoyancy, *J. Fluid Mech.* 26 (1966) 779–792.
- [18] J.S. Turner, Bouyant plumes and thermals, *Annu. Rev. Fluid Mech.* 1 (1969) 29–44.
- [19] W.D. Baines, J.S. Turner, Turbulent buoyant convection from a source in a confined region, *J. Fluid Mech.* 37 (1969) 51–80.
- [20] I.H. Campbell, J.S. Turner, Fountains in magma chambers, *J. Petrology* 30 (1989) 885–923.
- [21] W.D. Baines, J.S. Turner, I.H. Campbell, Turbulent fountains in an open chamber, *J. Fluid Mech.* 212 (1990) 557–592.
- [22] E.J. List, Turbulent jets and plumes, *Annu. Rev. Fluid Mech.* 14 (1982) 189–212.
- [23] H. Zhang, R.E. Baddour, Maximum penetration of vertical round dense jets at small and large Froude numbers, *J. Hydraulic Eng.* 124 (1998) 550–553.
- [24] P.D. Friedman, J. Katz, Rise height for negatively buoyant fountains and depth of penetration for negatively buoyant jets impinging an interface, *ASME J. Fluids Eng.* 122 (2000) 779–782.
- [25] L. J. Bloomfield, R.C. Kerr, Inclined turbulent fountains, *J. Fluid Mech.* 451 (2002) 283–294.
- [26] A. W. Woods, Turbulent plumes in nature, *Annu. Rev. Fluid Mech.* 42 (2010) 391–412.
- [27] W. Lin, S.W. Armfield, Direct simulation of weak axisymmetric fountains in a homogeneous fluid, *J. Fluid Mech.* 403 (2000) 67–88.

- [28] W. Lin, S.W. Armfield, Very weak fountains in a homogeneous fluid, *Numerical Heat Transfer: Part A: Applications* 38 (2000) 377–396.
- [29] W. Lin, S.W. Armfield, The Reynolds and Prandtl number dependence of weak fountains, *Comput. Mech.* 31 (2003) 379–389.
- [30] P. Phillipe, C. Raufaste, P. Kurowski, P. Petitjeans, Penetration of a negatively buoyant jet in a miscible liquid, *Phys. Fluids* 17 (2005) 053601.
- [31] J.A. Duffie, W.A. Beckman, *Solar Engineering of Thermal Processes (2nd Edn)*, John Wiley & Sons, New York, 1991.
- [32] H.C. Burridge, A. Mistry, G.R. Hunt, The effect of source Reynolds number on the rise height of a fountain, *Phys. Fluids* 27 (2015) 047101.
- [33] H.B. Fischer, E.J. List, R.C.Y. Koh, J. Imberger, N.H. Brooks, *Mixing in Inland and Coastal Waters*, Academic Press, New York, 1979.
- [34] T.S. van den Bremer, G.R. Hunt, Two-dimensional planar plumes and fountains, *J. Fluid Mech.* 750 (2014) 210–244.
- [35] L.J. Bloomfield, R.C. Kerr, Turbulent fountains in a stratified fluid, *J. Fluid Mech.* 358 (1998) 335–356.
- [36] G.R. Hunt, C.J. Coffey, Characterising line fountains, *J. Fluid Mech.* 623 (2009) 317–327.
- [37] H. Zhang, R.E. Baddour, Maximum vertical penetration of plane turbulent negatively buoyant jets, *J. Eng. Mech.* 123 (1997) 973–977.
- [38] D. Goldman, Y. Jaluria, Effect of opposing buoyancy on the flow in free and wall jets, *J. Fluid Mech.* 166 (1986) 41–56.
- [39] W. Lin, S.W. Armfield, Direct simulation of weak laminar plane fountains in a homogeneous fluid, *Int. J. Heat Mass Transfer* 43 (2000) 3013–3026.

- [40] N. Srinarayana, G.D. McBain, S.W. Armfield, W. Lin, Height and stability of laminar plane fountains in a homogeneous fluid, *Int. J. Heat Mass Transfer* 51 (2008) 4717–4727.
- [41] W. Gao, W. Lin, T. Liu, S.W. Armfield, Onset of asymmetry and three-dimensionality in transitional round fountains in a linearly stratified fluid, *Proc. 18th Australasian Fluid Mech. Conf.*, [Launceston, Australia](#), Paper-213 (2012).
- [42] [Y.A. Çengel, J.M. Cimbala, Fluid Mechanics - Fundamentals and Applications, McGraw-Hill, New York, 2006.](#)